

Thermal and exhumation history of the central Rwenzori Mountains, Western Rift of the East African Rift System, Uganda

F. U. Bauer · U. A. Glasmacher · U. Ring ·
A. Schumann · B. Nagudi

Received: 30 October 2009 / Accepted: 19 April 2010 / Published online: 4 June 2010
© Springer-Verlag 2010

Abstract The Rwenzori Mountains (Mtns) in west Uganda are the highest rift mountains on Earth and rise to more than 5,000 m. We apply low-temperature thermochronology (apatite fission-track (AFT) and apatite (U–Th–Sm)/He (AHe) analysis) for tracking the cooling history of the Rwenzori Mtns. Samples from the central and northern Rwenzoris reveal AFT ages between 195.0 (± 8.4) Ma and 85.3 (± 5.3) Ma, and AHe ages between 210.0 (± 6.0) Ma to 24.9 (± 0.5) Ma. Modelled time–temperature paths reflect a protracted cooling history with accelerated cooling in Permo-Triassic and Jurassic times, followed by a long period of constant and slow cooling, than succeeded by a renewed accelerated cooling in the Neogene. During the last 10 Ma, differentiated erosion and surface uplift affected the Rwenzori Mtns, with more pronounced uplift along the western flank. The final rock uplift of the Rwenzori Mtns that partly led to the formation of the recent topography must have been fast and in the near past (Pliocene to Pleistocene). Erosion could not compensate for the latest rock uplift, resulting in Oligocene to Miocene AHe ages.

Keywords Low-temperature thermochronology · Apatite fission-track · Uplift · Denudation · Rwenzori Mountains · Albertine Rift

Introduction

The main goal of this study is to unravel the cooling and uplift history of the Rwenzori Mountains (Mtns) southwest of Lake Albert in the western branch of the East African Rift System (EARS). With elevations reaching more than 5,000 m a.s.l. (metre above sea level), the eastern and western branches of the EARS (Fig. 1) comprise a markedly differentiated topography. Here, the highest mountains of Africa can be found. The Kilimanjaro (5,893 m a.s.l.) and Mt. Kenya (5,199 m a.s.l.) developed on the rift shoulders of the eastern branch and are both of volcanic origin. In the Albertine Rift of the western branch, however, the highest mountains occur within the rift proper and are built up by a Precambrian metamorphic basement block that has been uplifted to heights of 5,109 m a.s.l.—the Rwenzori Mtns (Fig. 1).

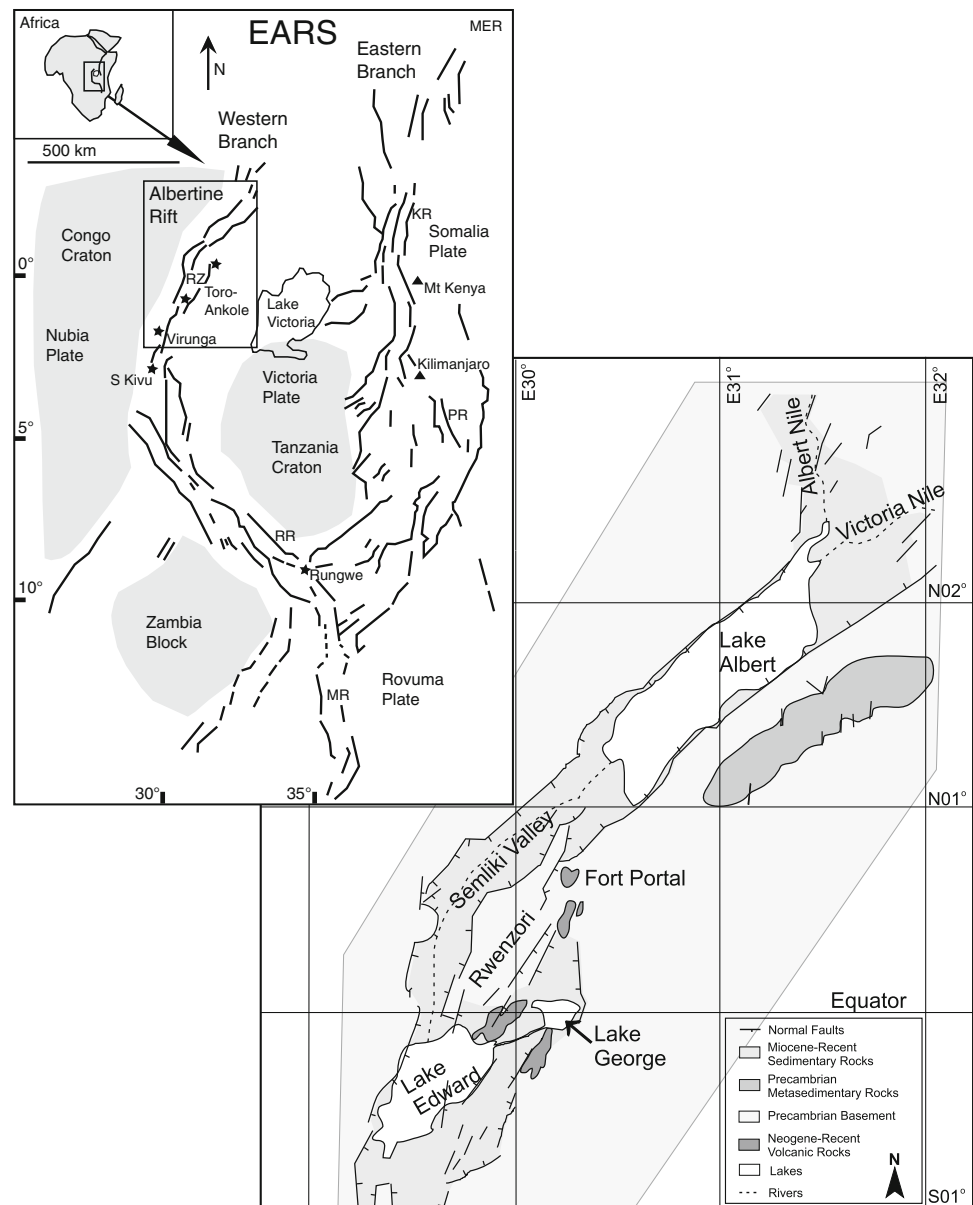
Located within an extensional setting and lacking any volcanic origin, the exceptionally high Rwenzori Mtns raise the question about their evolution and their linkage to the surrounding Albertine Rift. The interdisciplinary research project *RiftLink* (funded by the German Research Foundation, DFG) focuses on this issue by addressing rift dynamics, uplift, and climate change in Equatorial Africa. The prime subject of *RiftLink* is the Albertine Rift with the Rwenzori Mtns. A major issue of this study is to constrain the temporal evolution of the Rwenzori Mtns and to decipher if their elevation can be entirely ascribed to rift-related uplift in Neogene times, or if they formed a topographic high long before?

F. U. Bauer (✉) · U. A. Glasmacher
Institute of Earth Sciences, University of Heidelberg,
Im Neuenheimer Feld 234, 69120 Heidelberg, Germany
e-mail: Friederike.Bauer@geow.uni-heidelberg.de

U. Ring
Department of Geological Sciences, University of Canterbury,
Private Bag 4800, Christchurch 8140, New Zealand

A. Schumann · B. Nagudi
Geology Department, Makerere University,
P. O. Box 7062, Kampala, Uganda

Fig. 1 Top: Overview of the central part of the EARS with location of the Rwenzori Mtns in the Albertine Rift (adapted from Koehn et al. 2008). Old cratons and involved plates are outlined, as well as site of specific volcanic provinces (asterisk, triangle) and rift basins; RZ Rwenzori Mtns, RR Rukwa Rift, MR Malawi Rift, PR Pangani Rift, KR Kenya Rift, MER Main Ethiopian Rift. Enlarged illustration: Albertine Rift with simplified geological map, showing the Rwenzori Mtns, between Lake Albert and Lake Edward and Semliki Valley to the west (modified after Laerdal and Talbot 2002)



The evolution of a mountain range is generally marked by phases of topographic growth, equilibrium, and decay (Davis 1899; Ahnert 2003). Associated erosion rates vary in response to temporal and spatial changes in climate, topographic relief, topographic slope, and deformation (Kooi and Beaumont 1996; Bishop 2007). As rocks are exhumed through the Earth's crust, they cool through the thermal field from hot sub-surface temperatures to significantly colder surface temperatures (Reiners and Shuster 2009). Well-suited tools to track this cooling history are various low-temperature thermochronology methods, which yield the time at which the rock has passed through a certain isotherm (Batt and Brandon 2002; Reiners and Ehlers 2005; Lisker et al. 2009). Relevant information is stored in heavy minerals, such as apatite and zircon, and

can be revealed by different low-temperature thermochronology techniques. To unravel the temporal component in the evolution of the Rwenzori Mtns fission-track and (U–Th–Sm)/He analyses on apatites was applied. When exhumation is driven by active tectonic processes, thermochronological studies in combination with thermokinematic modelling provide estimates on the rates at which rocks are brought to the surface relative to the acting tectonic forces. This in turn allows deriving information on the behaviour of the coupled tectonic-erosion system (e.g. Kooi and Beaumont 1994, 1996; Bishop 2007).

In this paper, we present low-temperature thermochronological data, cooling histories, and provide exhumation rates and hints on the timing of the surface uplift of the Rwenzori Mtns in the western branch of the EARS, with

the terms surface uplift, rock uplift and exhumation of rocks used as defined by England and Molnar (1990).

Regional setting

The East African Rift System

In the long-established geological record of the African continent that spans at least 3.8 billion years, the East African Rift System (EARS) is a fairly young but very prominent structure. It ruptures through the East African swell and creates a horst and graben landscape with great escarpments (Petters 1991). Rifting processes in the EARS started in Palaeogene times and are still active. Two rift arms developed: the Eastern Rift (Gregory Rift) and the Western Rift, with the Albertine Rift forming the northernmost part of the Western Rift (Schlueter 1997, and references therein), (Fig. 1).

The Eastern Rift extends from the Afar region, north of the Main Ethiopian Rift, through Ethiopia and Kenya into Tanzania. It shows a southward propagation of the rift arm that started in Oligocene times (Nyblade and Brazier 2002). In general, the Eastern Rift is characterized by pronounced volcanic activity, with volcanic cones reaching heights of more than 5,000 m a.s.l. (Mt. Kenya and Kilimanjaro), and a broad regional elevation of the rift floor up to 2,000 m a.s.l. due to plume-related updoming (e.g. Ebinger and Sleep 1998).

The Western Rift extends along the western border of Uganda and Tanzania down to the Malawi Rift, and converges with the re-emergent Eastern Rift at the triple junction south of Tanzania (Schlueter 1997). A series of rift basins from the Lake Malawi Rift Basin in the south to the basins of Lake Edward, Lake George, Semliki and Lake Albert in the north is associated with the Western Rift (Ebinger 1989). In the following, the northern rift basins (Lake Edward Basin, Lake George Basin, Semliki Basin and Lake Albert Basin) will be collectively referred to as Albertine Rift (Fig. 1). Rifting in the Western Rift was initiated in Miocene times, with the rift developing to the north and south, linking originally isolated basins (Ebinger 1989; Morley 1999). Initial volcanic activity in the Western Rift started at ~ 12 Ma in the north and at ~ 7 Ma in the south and is restricted to the areas of Rungwe, Virunga, South Kivu and Toro-Ankole (Fig. 1) (Logatchev et al. 1972; Ebinger 1989; Kampunzu et al. 1998; Ebinger and Furman 2002). Compared to the Eastern Rift, the Western Rift shows minor volcanic activity, and minor regional elevation, but is characterized by deep rift lakes and steep fault scarps rising up thousands of metres adjacent to the graben floor. The highest of these fault scarps appears in the northern part of the rift, on the Rwenzori horst block,

where the Margherita Peak (5,109 m a.s.l.) rises to more than 4,000 m above the plains of Semliki River (Uccott et al. 1996; Schlueter 1997; Karner et al. 2000).

The Rwenzori Mtns

The Rwenzori Mtns represent a horst block within the Albertine Rift and are surrounded by deep rift valleys with Lake Albert to the north, Lake Edward to the south, the Semliki Valley to the west, and Lake George to the southeast (Fig. 1) (Bahat and Mohr 1987; Schlueter 1997; Karner et al. 2000). Made up by a dissected Precambrian metamorphic basement block the Rwenzori Mtns represent the highest non-volcanic mountain range in Africa.

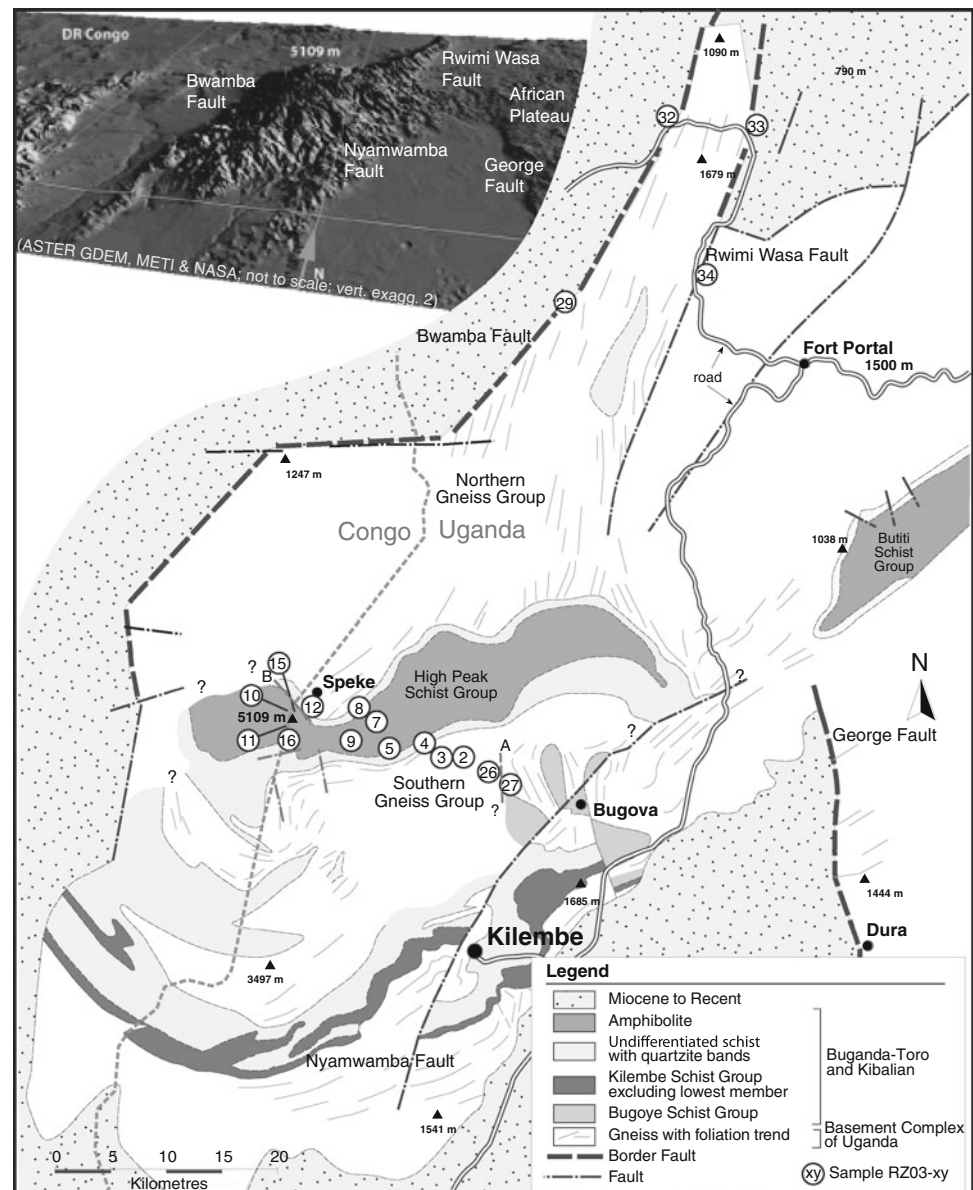
In general, the uplifted Precambrian basement along the rift shoulders of the Albertine Rift is covered by Cenozoic volcanic rocks and lateritic soils of unknown age. The rift basins are filled with fluvial, lacustrine, and minor volcanic material. Onland stratigraphic evidence along with recent well data from Lake Albert indicates that the oldest sediments in the Lake Albert Basin are Late Miocene in age (Pickford et al. 1993; Ovington and Burdon 2009).

The Rwenzori Mtns are predominantly characterized by bare rock faces, especially within the central part, where only the valleys are locally filled with Cenozoic detrital sediments, representing fluvio-glacial deposits. The main lithological units of the Rwenzori Mtns are gneisses, schists and amphibolites, subordinate intrusive rocks of various metamorphic overprint, and quartzite (e.g. Michot 1938; Tanner 1971; Nagudi et al., *in preparation*) (Fig. 2). The Precambrian rocks crop out in a complex tectonic setting, with all units intensively truncated by N–S, NW–SE, and E–W trending normal faults, locally with a significant strike-slip component (for more details cp. McConnell 1959; Ring 2008; Koehn et al. 2010).

The landscape evolution of the Albertine Rift and the Rwenzori Mtns are still poorly constrained and explanations for the high topography remain controversial, as well as assumptions concerning the timing of uplift (e.g. Pickford 1990; van Damme and Pickford 2003). Karner et al. (2000) and Ring (2008) showed that there is a relationship between the high topography in the central Rwenzori Mtns and the glaciations.

Structural, sedimentological and palaeontological studies suggest the following evolutionary stages for the Western Rift in general (Fig. 3): (1) Early faulting and subsidence in the area of the Albertine Rift occurred at ~ 18 – 20 Ma (Abeinomugisha and Mugisha 2004; Delvaux and Barth 2010); (2) initial volcanic activity affected the Virunga Province at ~ 12 Ma, prior or concurrent to initial faulting and subsidence of rift basins (Ebinger 1989); (3) tectonic movements at ~ 10 – 8 Ma were reported for Lake

Fig. 2 DEM and geological overview-map of the Rwenzori Mtns with sample locations; fault pattern of the central Rwenzori Mtns is indicated, with fault A (? exact trending of fault not known) and B discussed in the text (modified after Wallis and Valliant 2004; Koehn et al. 2008; Ring 2008); vertical exaggeration 2x

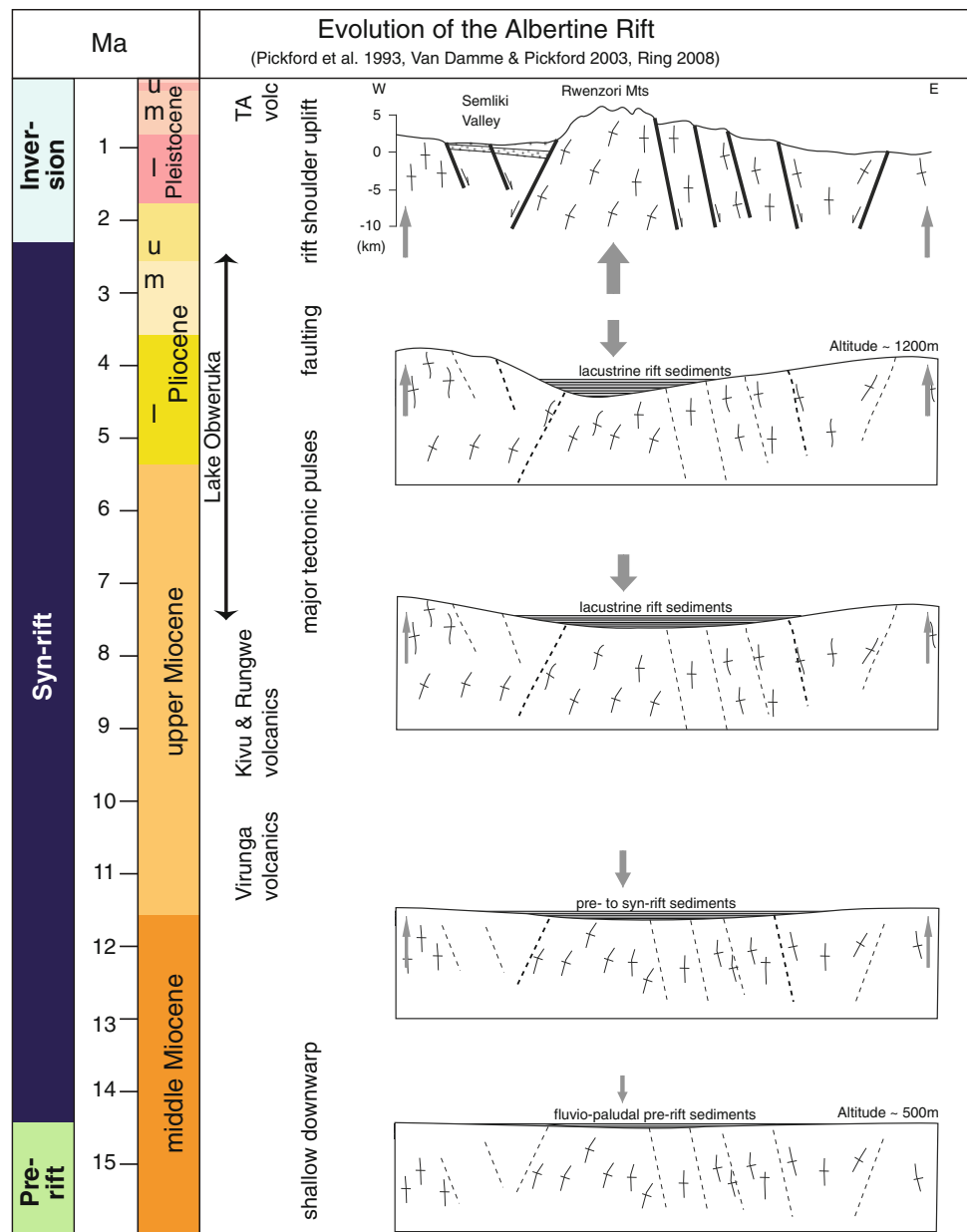


Kivu and Lake Albert rift basins, accounting for the diachronous evolution; (4) first major episodes of rifting started at $\sim 8\text{--}8.5$ Ma in the Albertine area with associated rift-flank uplift (Ring et al. 1992; Ebinger et al. 1993; Ring and Betzler 1995); (5) a second tectonic pulse and accompanied uplift affected the area of the Albertine Rift at $\sim 2\text{--}3$ Ma (cp. Pickford et al. 1993; Ring 2008). It is assumed that exhumation of the Rwenzori Mtns started at this time. Referring to Van Damme and Pickford (2003), an aerially extensive palaeo-lake (Lake Obweruka) existed from ~ 7.5 to 2.5 Ma and covered the entire area of the Albertine Rift for most of that period. Due to a major tectonic pulse, this palaeo-lake was separated into present Lake Albert and Lake Edward at ~ 2.5 Ma. It is supposed that this pulse was associated with a period of rifting and

footwall surface uplift that finally led to the surface uplift of the rift shoulders and the Rwenzori Mtns, and associated tilt of the rift basins (Ebinger 1989; Pickford et al. 1993; Taylor and Howard 1998).

The Rwenzori Mtns are truncated by various fault systems dissecting the mountain range into several blocks. At least three recurring fault sets that are overprinting each other can be observed in the central Rwenzori Mtns (Ring 2008). The western boundary of the Rwenzori Mtns is made up by the large-displacement Bwamba border fault, whereas the eastern side of the Rwenzori Mtns is controlled by the Rwimi-Wasa fault in the north and the Nyamwamba fault in the south (Fig. 2). In addition, the seismically active central part of the Rwenzori Mtns is dissected by fault sets striking E–W, N–S and NW–SE (Ring 2008,

Fig. 3 Schematized evolution of the Albertine Rift basin with major phases of tectonic and volcanic activity and indicated sedimentary evolution (modified after Pickford et al. 1993; Van Damme and Pickford 2003; Ring 2008). Volcanism in the Western Rift started at ~12 Ma in Virunga, ~8–9 Ma in the Kivu and Rungwe volcanic fields, and ~70 ka in the Toro-Ankole province (TA volc.) (Kampunzu et al. 1998; Boven et al. 1998), cp. Fig. 1 for location



Koehn et al. 2008). The numerous valleys that are dissecting the Rwenzori Mtns into several blocks predominantly are fault-related, following pre-existing tectonic structures (Bauer et al., in review).

Geomorphology of the Rwenzori Mtns

The Rwenzori Mtns, with a lateral dimension of about 120 km NS and 50 km EW, show a recent topography reaching from about 1,000 m a.s.l. to 5,109 m a.s.l.. From N to S different areas can be distinguished giving the Rwenzori Mtns their remarkable shape: the long and narrow northern range, the central to south-central high-peak area, with the highest elevations and broadest widths that

gradually merges into the southern part with decreasing widths and altitudes (cp. Fig. 2). Apart from a small connection to the craton at their north-eastern flank, the entire Rwenzori Mtns are enclosed by the rift valley.

As described, e.g., by Whittow (1966); Ollier and Pain (2000); Osmaston and Harrison (2005), the present relief of the Rwenzori Mtns bears witness of several glacial cycles. Above ~2,500 m a.s.l., the evolution of topography is strongly influenced by large Pleistocene and Holocene ice sheets, whereas inherited fault systems and prevailing rock composition pave the way for erosion. The peaks are shaped by erosion, with glaciers still covering the top (Fig. 4). The initial landscapes were probably created by fluvial erosion and remodelled by glaciation (Ollier and



Fig. 4 Landscape in the high mountain ranges of the central Rwenzori Mtns. Top pictures: Glaciated peaks of the Rwenzoris, Mt Margherita (*left & middle*), Mt Baker (*left*). Bottom: Glacial forms at ~3,000–4,500 m. Traces of pre-glacial landscapes are still visible

Pain 2000), as indicated by wide U-shaped valleys (Fig. 4). Currently, two main rivers dewater the central Rwenzori Mtns to the east into Lake George, with recent erosion rates ranging between 35 and 140 mm/ky, with largest values of 115 and 140 mm/ky at their steeper south-eastern flank (Roller et al. 2008).

The erosion rates constrained by Roller et al. (2008) represent a more recent snapshot and because of the glacial cycles long-term erosion rates may have been different. Long-term erosion rates in mountain chains are commonly estimated by integrating over a full glacial/interglacial cycle (or better a few of them) to average out short-term (100–1,000 year scale) variability in climate and sediment accumulation rates (Burbank, pers. comm., 2009). Long-term erosion rates are thus on the $\geq 100,000$ year time scale.

The landscape in the central Rwenzori Mtns has threshold slopes ($\sim 30^\circ$), i.e. slopes that are at the limit of Coulomb failure. In these landscapes, the erosion rates are only dependent on rock uplift (Montgomery and Brandon 2002). When threshold slopes are present, the topographic system has to be at steady state, i.e. rock uplift equals erosion. The landscape in the Rwenzori Mtns is similar to landscapes in the Southern Alps of New Zealand, the Himalaya or other active, deeply incised mountain belts on Earth that have long-term erosion rates $> \sim 0.5$ mm/year.

Erosion in the Rwenzori Mtns occurs to a great degree by landslides. The landslides are in turn masked by heavy vegetation but at their head scarps there is fresh outcrop along slopes of valleys which are otherwise characterized by glacial debris. The fresh outcrop in the Rwenzori Mtns, also at its high peaks, shows that uplift and exhumation processes there must be fundamentally different than at the other rift flanks in the East African Rift where rocks are typically deeply weathered and form Miocene land

within narrow valleys and sharp cliffs with scree slopes (*right*). In other parts glaciation has removed much more material, resulting in wide valleys, with scree covered by organic material, giving way for vast swamps or bogs (*middle*) within u-shaped valleys (*left*)

surfaces indicating that they were eroded and exhumed very slowly. Big landslides also obscure the glacially formed landscape in the Rwenzori Mtns, as they do in other active, glacially formed landscapes.

As commonly observed in mountains of glaciated areas that do not collect snow, broad parts of the Rwenzori Mtns are attacked by frost, giving rugged mountains, and steep rock upper slopes over scree-covered lower slopes. Feral mountain landscapes often result from incised rivers and are an indicator for active uplift (e.g. Ollier and Pain 2000). The central high peak area of the Rwenzori Mtns is an example for such morphotectonic interactions. Sections across the Rwenzori Mtns, derived from digital elevation models (DEM), illustrate the course of topography along- and across-axis (Fig. 5). The delineated compensating curve of section 1, Fig. 5 traces the expected course of topography wavelength along axis and cuts through the high peaks of the central Rwenzori Mtns. This is pointing to a more pronounced surface uplift of the central part, in respect to the flanking areas, with an associated erosion surface, as derived from field observations (Bauer et al., *in review*). Further structural as well as morphologic features of the Rwenzori Mtns can be observed across-axis. Following WNW–ESE trending cross-sections, the slopes are much steeper on the western part of the Rwenzori Mtns than to the east. This asymmetry is most striking in the central part, where the western flank locally rises from about 1,000 m a.s.l. to heights of more than 4,500 m a.s.l. within less than 15 km, whereas the eastern flank plunges along a distance of more than 30 km to reach 1,000 m a.s.l. again (Fig. 5, section 2). The western flank is sharp bounded against the adjacent rift valley by the Bwamba fault, showing more pronounced fault scarps (cp. Fig. 2). The eastern flank, however, is lacking a clear and continuous bounding fault

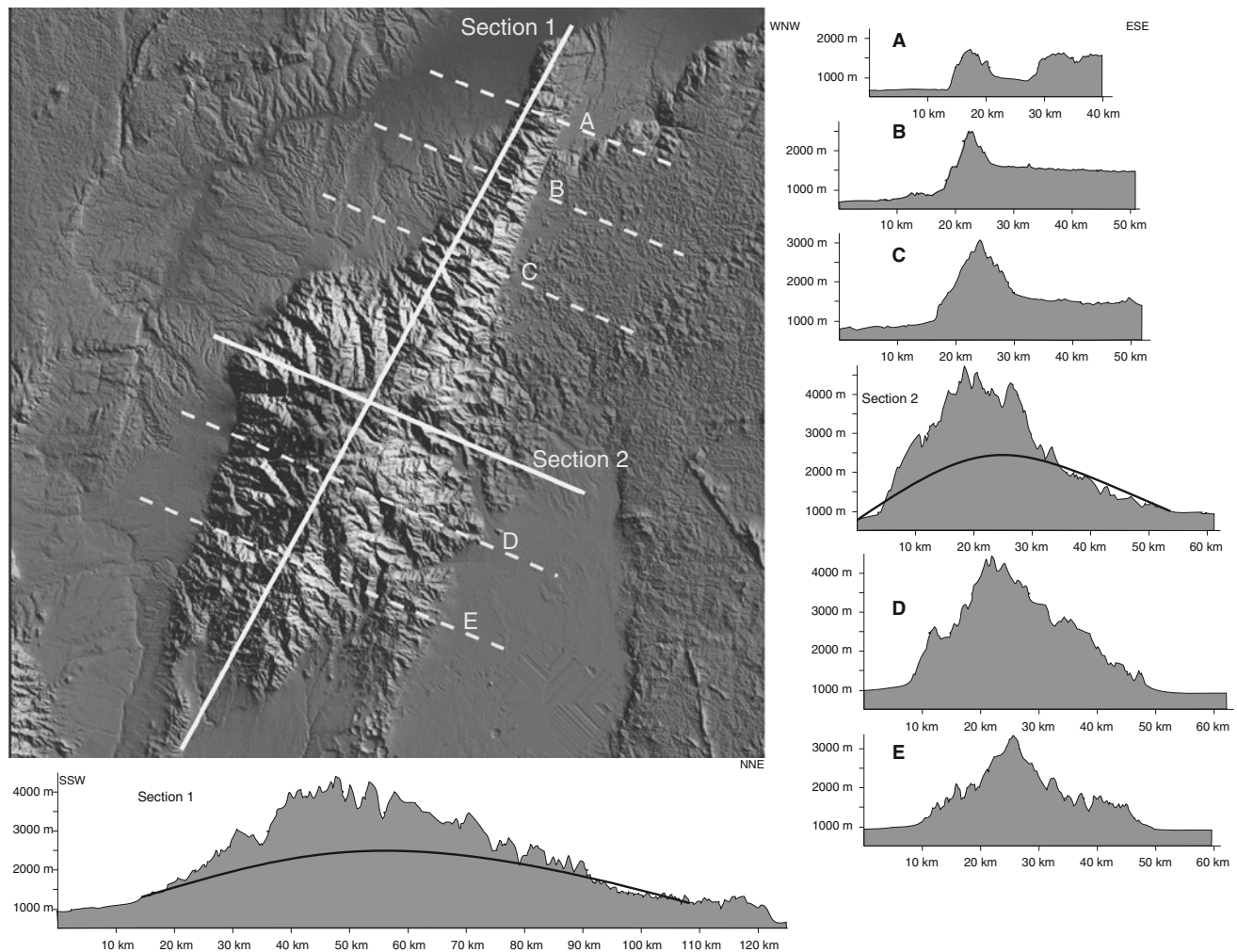


Fig. 5 DEM of the Rwenzori Mtns with several cross-sections along and across the Rwenzori Mtns, revealing a highly dissected morphology. *Section 1* SSW–NNE oriented section, showing successive increase in altitudes from NNE towards high peaks, highest elevations in the central Rwenzoris followed by a slightly steeper drop in altitudes towards SSW; drawn compensating curve illustrates an idealized trending of topography wavelength cutting through the

high peaks. *Section 2* WNW–ESE section across the central high peak area demonstrates the W–E asymmetric character of the Rwenzoris; comparable to *section 1* the compensating curve cuts the high peaks of the central part. Additional cross-sections (A–E) further illustrate the asymmetry and the more pronounced fault scarp along the western flank. See text for further interpretation

as it is still connected to the African Plateau along a distance of about 60 km.

Thermochronology in the EARS

Only a few thermochronological studies quantify the cooling, uplift and denudation history of the rift flanks within the EARS (Fig. 6). These studies are mainly related to the Afar region, and Kenya and Tanzania rifts of the eastern rift branch, as well as the Malawi and Rukwa Rift flanks of the western branch (Figs. 1, 6). These studies used apatite fission-track, titanite, zircon and apatite (U–Th–Sm)/He analysis and reported different stages of denudation within the EARS. On the base of apatite fission-track data, e.g. van der Beek et al. (1998) concluded that

the Malawi and Rukwa Rifts record a protracted cooling and exhumation history with an old stage around 250–200 Ma (2.0 ± 0.4 km denudation), a second at about 150 Ma (2.0 ± 0.4 km denudation) and a third stage during Cenozoic time ($\leq 1.2 \pm 0.2$ km denudation). AFT data recorded at the Livingstone Escarpment (Malawi Rift) reveal a Cenozoic exhumation history with more than half of the denudation taking place since 20 Ma (van der Beek et al. 1998). Comparable timing is reported for the Kenya and Tanzania Rift flanks (Foster and Gleadow 1992, 1996; Wagner et al. 1992; Mbede 2001; Spiegel et al. 2004, 2007). Spiegel et al. (2007) also found three major cooling episodes in the Kenya Rift: (1) during the Early Cretaceous, (2) the Late Cretaceous, and (3) the late Neogene, with intermittent periods of slow to very slow cooling.

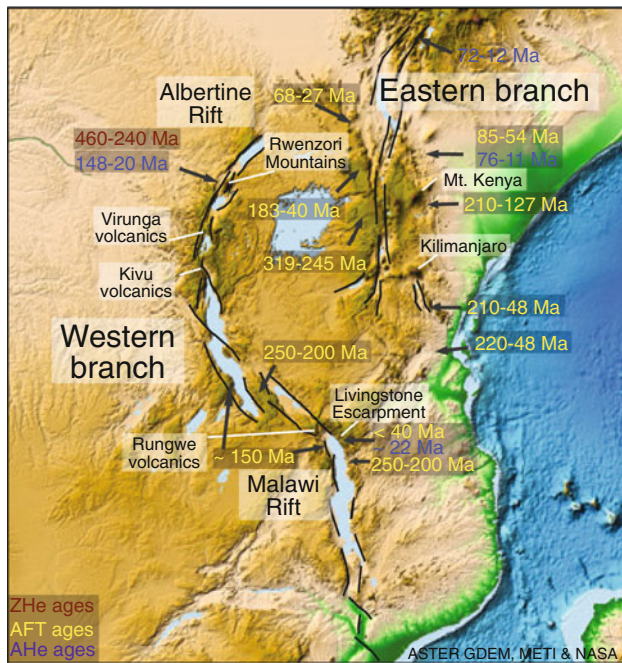


Fig. 6 Locations of thermochronological studies in the EARS with accordant apatite fission-track (AFT, yellow) and (U–Th–Sm)/He ages from apatite (AHe, purple) and zircon (ZHe, red). See text for more details and studies of: Abbate et al. (2002); Foster and Gleadow (1992, 1996); MacPhee (2006); Mbede (2001); Noble et al. (1997); Pik et al. (2003, 2008); Spiegel et al. (2004, 2007); van der Beek et al. (1998); Wagner et al. (1992)

In contrast to the punctuated cooling history reported for large parts of the EARS, Pik et al. (2008) reveal a continuous rift development since rift initiation in Miocene times about 20 Ma ago for the Ethiopian part of the EARS.

For the Rwenzori Mtns there is only one study known so far, applying thermochronological techniques. Apart from apatite-, zircon-, and titanite U–Pb ages, MacPhee (2006) acquired zircon and apatite (U–Th–Sm)/He data (ZHe, AHe). The spectrum of cooling ages (ZHe and AHe) shows a wide spread, with AHe ages (7) ranging between 262.5 (± 6.39) Ma and 18.9 (± 0.5) Ma (elevations: 690 m to 4,620 m a.s.l.). Despite the differences in sampled altitude, no age elevation relationship was observed by MacPhee (2006).

Methods

Thermochronologic methods, such as (U–Th–Sm)/He and fission-track (FT) dating, are based on the production of an isotope or radiation damage, resulting from nuclear decay, and the subsequent, thermally controlled retention of these decay products. As described, e.g., by Reiners and Brandon (2006), the radioisotopic production decreases exponentially with time but is predictable and otherwise steady,

which gives the thermochronometer the ability to keep time. Due to the thermal sensitivity of thermochronometers, thereof revealed ages provide information about the cooling history of the rock, rather than the crystallization ages of its minerals (although in some cases they do record crystallization ages as well).

To resolve the thermal evolution of the Rwenzori Mtns, apatite fission-track (AFT) and apatite (U–Th–Sm)/He analyses (AHe) were performed. Whenever possible both thermochronometers were applied to the same sample, allowing a more robust evaluation of the spatial and temporal cooling of the samples. Thermal modelling was used to determine the cooling histories of individual samples and trace their exhumation through the upper crust.

For this study, 21 samples were processed for thermochronological analyses, with 15 samples yielding enough apatite grains for the analytical work. The majority of samples was taken from the eastern flank of the central Rwenzori Mtns along an E–W transect (17 samples), and some spot samples were taken from the northern Rwenzori Mtns (4 samples) (Fig. 2). The sampled lithologies are mainly Precambrian granitic gneisses, amphibolites, sillimanite-muscovite-biotite schist, quartz-biotite schist, garnet-muscovite schist, and quartzites (Fig. 2). The elevations range from ~ 800 m a.s.l. at the foothills to $\sim 4,800$ m a.s.l. at the high peaks of the Rwenzori Mtns.

To extract apatite crystals, the collected samples were processed following the general heavy mineral separation routine (cp. Donelick et al. 2005, and literature cited therein). In some lithological units, apatite crystals are scarce, usually very small and/or of poor quality. At least one-third of the treated samples are loaded with sillimanite, and some of them do not yield sufficient apatite grains for AFT and/or AHe analysis. Thus, AFT and AHe analytic were not applicable for all samples, and 6 samples could not be analysed.

Apatite fission-track thermochronology

The basic concept of the AFT method is the spontaneous fission of ^{238}U , during which the heavy fragments of this fission leave chemically etchable latent tracks in minerals and natural glasses (Wagner 1972). Information on the thermal history of apatite is stored in two archives: the etch pit areal density at an artificially polished internal surface, and the length distribution of horizontal confined tracks (e.g. Wagner and Van den haute 1992; Lisker et al. 2009, and literature cited therein). Fission of ^{238}U generates spontaneous fission-tracks that are metastable in relation to temperature. The temperature-sensitive annealing of fission-tracks in apatite is constraint by two important effects (1) the crystallographic orientation of the spontaneous tracks, and (2) the chemical composition of the apatite.

Tracks orthogonal to the *c*-axis anneal more rapid than tracks parallel to the *c*-axis (Green and Durrani 1977; Green 1981, 1988; Laslett et al. 1984; Donelick et al. 1999). Total annealing temperature of FT in apatite is governed by the fluorine- (90–110°C/10 Myr) and chlorine content (110–150°C/10 Myr). The partial annealing zone (PAZ) of FT's in apatite range down to 60°C/10 Myr. Annealing below 60°C is still considered to be minor for 100 Myr time ranges. The change of arithmetic mean fission-track etch pit size parallel to the crystallographic *c*-axis (kinetic parameter D_{par}) is depended on the chemical composition and the etching conditions (5.5 N HNO₃, 20 s, 21°C) (Sobel and Seward 2010, and literature therein).

Apatite fission-track analysis

Following the standard techniques for heavy mineral separation, as e.g. described by Grist and Ravenhurst (1992a, b), Donelick et al. (2005), apatite grains of 15 samples were prepared for AFT analysis of this study. The AFT grain mounts were etched in 5.5 N HNO₃ for 20 (±1) s at 20 (±1)°C and afterwards covered by U-free detection muscovite. The covered grain mounts, as well as two Durango apatite age standards and three glass neutron dosimeter (CN5, top, middle, and bottom of sample batch) were irradiated at the research reactor FRM II, Munich. After irradiation, the detection mica were etched in 48% HF for 20 (±1) min at 20 (±1) °C.

AFT data acquisition was performed in the laboratory of the Thermochronology and Archeometry research group at the University of Heidelberg. The FT-1 system used, consists of an Olympus® 'BX50' optical microscope, equipped with an Autoscan® 'AS3000i' 3-axis microscope stage, a high-resolution Peltier-cooled colour CCD camera 'ColorView III' (5 mega pixel) of Olympus®, connected to a computer unit. To increase the precision of stage movement, each axis is upgraded with an external laser scale sensor ('BL 55 RE' of Sony®), which guarantee a deviation of less than 500 nm along 4–5 cm of movement. The entire setup is operated through the Autoscan® software Trackscan®, which also calculates the track densities. Applying the largest possible resolution, each pixel is equivalent to less than 250 nm in size. Area densities were counted by using a 50x dry objective, whereas D_{par} (D_{par}^{\otimes} , etch pit size parallel to the *c*-axes) and confined fission-track length together with their individual angle relative to the *c*-axes were determined by using the Olympus set up with a 100x dry objective and the Autoscan® computer code 'EasyLength®'. AFT ages were calculated applying the ζ -method (external detector method as described by Hurford and Green (1982, 1983)). The ζ -value of 351.74 (±10.39) a/cm² was obtained by counting Durango apatite

age standards. All ages, 1 σ -errors, and radial plots were determined by using the computer code 'Trackkey' (Dunkl 2002), with the resulting data presented according to the recommendations of Hurford (1990).

Apatite (U–Th–Sm)/He thermochronology

The AHe thermochronology is based on the accumulation of ⁴He during the α -disintegration of ²³⁸U, ²³⁵U, ²³²Th, their daughter products and ¹⁴⁷Sm. The closure temperature (T_c) of mineral grains is dependent on: activation energy (E_a), a geometric factor for the crystal form (A), thermal diffusivity (D_0), the length of the average diffusion pathway from the interior to the surface of the grain (a) and the cooling rate at closure temperature (dT/dt) (Dodson 1973). In general, the apatite T_c is in the range of 70 ± 7°C for a simple monotonic cooling rate of 10°C/Myr, a subgrain domain size > 60 μm , an activation energy (E_a) of about 36 kcal/mol, and a $\log(D_0)$ of 7.7 ± 0.6 cm²/s (Farley 2000). Alpha (α) particles are emitted with high kinetic energy during decay of U and Th, and travel significant distances before coming to rest, which in turn poses a complication for the He dating method, as α -particles may be ejected out of the crystal being dated or injected into the crystal from decay occurring in surrounding grains. Therefore, a correction has to be applied for the loss/gain of radiogenic He generated within an outer rim of the mineral grain by the α -stopping distances (apatite: 25 μm) (Wolf et al. 1996; Farley et al. 1996; Farley 2000). While the α -ejection correction is applied more routinely, the recently introduced correction for radiation damage is still in progress (Shuster et al. 2006; Shuster and Farley 2009; Flowers et al. 2006; Flowers et al. 2009). Shuster et al. (2006) noted that ⁴He diffusion in apatite is impeded by radiation-induced damage to the crystal structure. Their ⁴He production-diffusion model predicts that the effective ⁴He closure temperature of apatite will vary with cooling rate and effective uranium concentration (eU) and may differ from the commonly assumed T_c of ~75°C/1 Myr by up to ±15°C (Shuster et al. 2006; Shuster and Farley 2009). To account for the accumulation of crystal defects due to the radioactive decay the eU factor (eU = [U] + 0.235 [Th], concentrations in weight %) was introduced (Shuster et al. 2006). This factor characterizes the dependency of ⁴He diffusion on the amount of accumulated crystal defects created by the movements of the fission products and the alpha-recoil nucleus' in the crystal lattice.

Apatite (U–Th–Sm)/He analysis

The heavy mineral separation follows the same procedure as applied for AFT analysis. The final evaluation of appropriate grains for the AHe technique, however, is more

restrictive, since the analytical work requires well-defined apatite crystals without any cracks, mineral or fluid inclusions. For this study, the heavy-mineral concentrates obtained from separation process were screened for suitable apatite grains. Thereof 13 samples were considered as applicable and accordant apatite crystals were picked. At least two grains per sample were selected, but whenever the quality of the sample allowed it three or more apatite grains were picked. Subsequently the crystal sizes were measured prior to the analysis.

The analytical work was performed at Kline Laboratory, Yale University (later at the Arizona Radiogenic Helium Dating Laboratory). He degassing of single apatite crystals was performed by a Nd:YAG laser. The quantification of the amount of He was done with a Balzers quadrupole mass spectrometer (QMS). Thereafter, U–Th–Sm content of the degassed crystal was measured on a high-resolution Element2 ICP-MS, with the obtained AHe data afterwards corrected for α -ejection (for further details on the (U–Th–Sm)/He analytical technique see Mitchell and Reiners 2003; Reiners and Nicolescu 2006).

Thermal modelling: t–T paths

A tool for testing various geological models of time–temperature (t–T) evolution of a specific area (crustal segment) under investigation is provided by the computer code HeFTy (Ketcham 2005; Ketcham et al. 2007a, b, 2009). The HeFTy algorithm considers known FT annealing kinetics and He-diffusion behaviour of apatite and zircon, and tests cooling and reheating scenarios against determined thermochronological data. Time–temperature constraints (t–T coordinates) revealed from the known geological evolution of the area have to be taken into account. Both forward and inverse modelling can be performed, constructing possible t–T paths that are in agreement with the observed thermochronological data set.

For this study AFT data were used. The determined AFT data set comprises single grain cooling ages, confined FT length distribution and etch pit length (i.e. D_{par}) as proxy for the chlorine and fluorine content of the individual apatite crystal.

In a first step, the FT data were modelled in a forward approach, considering information from geological evolution of the study area and determined AHe ages. The resulting t–T path provides one solution for a possible cooling history of the area. Based on the best forward model, the inverse modelling was initiated. Along the t–T path several constraint-boxes can be set, acting as starting fields for the inverse model. The software algorithm connects the fields to t–T paths and searches within the field for possible solutions. In a Monte Carlo approach, the computer code attempts to find out of 20,000 single t–T

paths, those ones that best approximate the measured data. The primary goal of the program is to define envelopes of good and acceptable results in t–T space that contain all paths passing baseline statistical criteria and that are conform to user-entered geological constraints. A good fit (displayed purple in graph) corresponds to a merit value of 0.50 or higher (goodness of fit, $\text{GOF} \geq 50\%$). This is the expected value if the time–temperature path and kinetic model are in fact the correct ones. An acceptable fit (displayed green in graph) corresponds to a merit value of 0.05 or higher ($\text{GOF} \geq 5\%$), indicating that the model has not failed the null hypothesis test that forms the basis of the applied statistics (Ketcham 2009; Ketcham et al. 2009).

To approach the most likely cooling history (best fit t–T path), the constraint boxes are opened up more widely in the first model runs and adapted successively to increase the amount of good fits and get the best solution.

In the case of the Rwenzori Mtns data, two general geological evolution models were tested. One that assumed a steady cooling history and a second one that allowed reheating and cooling. Reheating would simulate either subsidence or increased heat flow for a certain time interval. In all cases, no solution for the reheating and cooling model could be achieved. Therefore, solely the steady cooling models will be presented and discussed.

Results

Apatite fission-track age distribution

The 15 AFT central ages show a large range in ages, between 85.3 (± 5.3) Ma (RZ03-29) and 195.0 (± 8.4) Ma (RZ03-33) (Fig. 7; Table 1). All AFT ages are younger than the corresponding intrusion and metamorphic age of the rocks. The youngest AFT age was revealed from a granitic gneiss located at the western flank (1,230 m a.s.l.) of the northern Rwenzori Mtns, while the oldest age was obtained from a granite sample (RZ03-33) taken at the eastern flank of the northern Rwenzori Mtns (1,070 m a.s.l.). A comparable old age of 185.3 (± 8.3) Ma (RZ03-15) was found in the central Rwenzori Mtns at an elevation of 4,050 m a.s.l. Except for one sample (RZ03-02) all single grain age distributions pass the χ^2 -test ($P(\chi^2) > 5\%$) (Table 1). With respect to the 1σ -error of single grain ages, this indicates a homogenous single grain age distribution (Galbraith 1981).

In the central part of the Rwenzori Mtns, samples were taken along a ~ 35 km long SE–NW transect that covers elevations from 1,650 m a.s.l. to 4,800 m a.s.l. The central AFT ages range between 89.2 (± 4.9) Ma (RZ03-27) and 185.3 (± 8.3) Ma (RZ03-15). Most of the apparent ages scatter around 130 Ma and do not vary significantly with

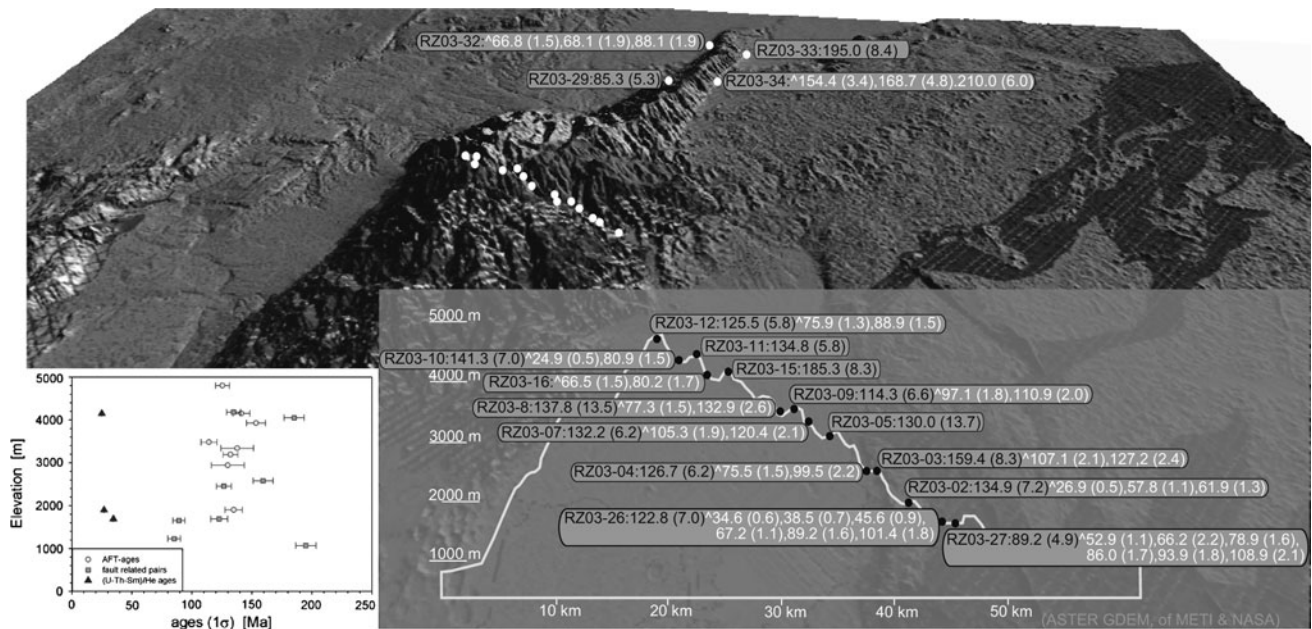


Fig. 7 Sample localities of the central and northern Rwenzori Mtns (view from S to N) with schematic transect to the right and age-elevations plot to the left to illustrate the independence of ages with

elevation. Within error, sample RZ03-26 from the lowest elevation (1,690 m a.s.l., 122.8 (± 7.0) Ma) has the same apparent age as the sample from the highest elevation (4,800 m a.s.l., 125.5 (± 5.8) Ma) (Fig. 7).

In the northern part of the Rwenzori Mtns, only two samples revealed enough grains for AFT analysis. The sample (RZ03-29, 1,230 m a.s.l) from the western flank yielded an AFT age of 85.3 (± 5.3) Ma, while the sample from the eastern flank (RZ03-33, 1,070 m a.s.l) revealed an AFT age of 195.0 (± 8.4) Ma.

Etch pit size

3,145 D_{par} values (etch pit size) were determined for all apatite grains processed in this study (Table 2). The D_{par} values show a narrow range between 1.4 (± 0.2) μm and 2.0 (± 0.5) μm . Referring to the lithologies and corresponding mean D_{par} values, a decrease from pegmatite (2.0 ± 0.5) to granites (1.5 ± 0.3) can be observed with gneiss lithologies (1.7 ± 0.3) and the amphibolite (1.8 ± 0.5) taking an intermediate position.

With the exception of samples RZ03-10 (−0.12) and RZ03-11 (−0.27), all samples exhibit a positive skewness between 0.06 and 1.58. The large skewness values indicate a larger variation in etch pit size. The largest etch pit size of 3.6 μm was measured in apatites from a granite-gneiss (RZ03-26). This sample also shows the largest spread in D_{par} values between 1.1 μm and 3.6 μm (± 0.3 μm). Within errors, no correlation has been detected between the single grain ages, the confined length and the D_{par} values.

altitude. Samples and AFT ages displayed black, AHe ages (marked with ^) are displayed white

Track length distribution

Eleven of the analysed FT samples yield more than 60 confined fission-tracks (CT) (Table 2). The obtained mean lengths of confined spontaneous fission-tracks range between 10.7 (± 1.5) μm and 12.1 (± 1.3) μm . 1,236 track lengths were measured. Apart from three exceptions (RZ03-03: 0.08; RZ03-08: 0.47; RZ03-26: 0.10), all other samples show a negative skewness between −0.01 and −0.77 indicating a trail of short tracks, which points to a complex cooling history. No correlation exists between track length distribution and elevation or variation of determined AFT ages. The 11 samples with more than 60 confined tracks were used for thermal modelling.

The measured confined spontaneous FT lengths were corrected for their crystallographic orientation using the computer code HeFTy (c-axis corrected fission-track length, L_c). The mean confined spontaneous fission-track length changed to a distribution between 12.6 (± 1.7) μm and 13.7 (± 1.1) μm . Except for sample RZ03-08 (L_c skew: 0.07), all samples show a negative skewness ranging from −0.05 to −1.53. Even with this correction no correlation exists between track length distribution and elevation or variation of FT ages.

Apatite (U–Th–Sm)/He age distribution

For the apatite (U–Th–Sm)/He analysis (AHe), 13 samples with 2–6 grains each were measured. Accordant results are summarized in Table 3 and illustrated in Fig. 7. The age

Table 1 Summary of apatite fission-track data and sample location with description

Sample	Elev. (m a.s.l.)	Lat.	Long.	Lith.	U (std) ($\mu\text{g/g}$)	n	Sp. tracks ρ_s N_s	Ind. tracks ρ_i N_i	P (χ^2) (%)	Central age $\pm 1\sigma$ (Ma)
Northern Rwenzori Mtns										
RZ03-29*	1230	0.70215	30.08990	gr-gn	9.0 (4.8)	19	3.627 460	10.771 1366	86.2	85.3 \pm 5.3
RZ03-32	800	0.83961	30.17127	peg	–	–	–	–	–	–
RZ03-33****	1070	0.83433	30.23498	gr	22.0 (16.2)	20	20.569 2053	24.026 2398	99.7	195.0 \pm 8.4
RZ03-34	1570	0.72379	30.19018	gr-gn	–	–	–	–	–	–
Central Rwenzori Mtns										
RZ03-02**	1900	0.36008	30.01423	peg	67.6 (11.5)	11	43.18 2472	81.566 4669	0.03	134.9 \pm 7.2
RZ03-03*	2580	0.36031	29.98516	gr-gn	6.2 (2.6)	28	4.684 917	7.437 1456	99.7	159.4 \pm 8.3
RZ03-04**	2450	0.36673	29.98379	gr-gn	12.5 (6.3)	20	7.760 1023	15.482 2041	100.0	126.7 \pm 6.2
RZ03-05****	2940	0.36794	29.95636	amp	2.5 (2.4)	10	1.803 153	3.24 275	100	130.0 \pm 13.7
RZ03-07****	3190	0.38054	29.94305	gr	17.4 (6.4)	22	11.405 1291	20.204 2287	99.8	132.2 \pm 6.2
RZ03-08*	3340	0.38898	29.93441	gr	23.3 (16.5)	15	16.708 199	31.233 372	37.8	137.8 \pm 13.5
RZ03-09***	3480	0.38325	29.92950	gr-gn	7.6 (3.5)	20	4.285 607	9.932 1407	98.5	114.3 \pm 6.6
RZ03-10**	4150	0.39178	29.88243	gr-gn	12.6 (4.6)	18	9.475 1032	16.93 1844	100.0	141.3 \pm 7.0
RZ03-11****	4180	0.37997	29.87586	gr-gn	19.6 (4.8)	18	13.655 1778	23.301 3034	99.9	134.8 \pm 5.8
RZ03-12***	4800	0.40800	29.89221	gr-gn	15.9 (6.7)	22	10.687 1252	22.544 2641	99.8	125.5 \pm 5.8
RZ03-15*	4050	0.37858	29.88791	bt-gn	37.2 (20.6)	22	34.812 2339	47.403 3185	17.4	185.3 \pm 8.3
RZ03-16	4150	0.37557	29.88462	bt-gn	–	–	–	–	–	–
RZ03-26***	1690	0.34613	30.03796	gr-gn	5.8 (3.4)	21	3.544 632	7.655 1365	100.0	122.8 \pm 7.0
RZ03-27***	1650	0.34086	30.04473	gr-gn	20.2 (14.1)	20	8.936 883	26.716 2640	36.9	89.2 \pm 4.9

Sample-Location: Elevation in metre above sea-level, Latitude and Longitude (UTM coordinates, WGS 84); Lith.: lithology; peg: pegmatite, gr-gn: granitic gneiss, bt-gn: biotite gneiss, gr: granite, amp: amphibolites; U (std): Uranium concentration and standard deviation in $\mu\text{g/g}$; n: number of counted apatite grains; ρ_s : density of spontaneous tracks (10^5 tr/cm^2), N_s : number of spontaneous tracks; ρ_i : density of induced tracks (10^5 tr/cm^2), N_i : number of induced tracks; $P(\chi^2)$: probability that single grain ages are consistent and belong to the same population. Test is passed if $P(\chi^2) > 5\%$ (Galbraith 1981). Ages are calculated using a ζ -value of $351.74 \pm 10.39 \text{ a/cm}^2$; tracks counted on CN5 dosimeter glass (Nd) are marked by *: Samples with *: Nd = 18367 tracks, with **: Nd = 14796 tracks, with ***: Nd = 15471 tracks, with ****: Nd = 10118 tracks

variation of the α -ejection corrected single grain ages range between 210.0 (± 6.0) Ma and 24.9 (± 0.5) Ma. Within one sample (RZ03-27) of 6 grains, the corrected single grain ages vary between 108.9 (± 2.1) Ma and 52.9 (± 1.1) Ma. A

correlation between apatite grain sizes and age distribution could not be revealed. The accumulation of radiation damage, however, which can be detected by the effective U concentration (eU) seems to have an effect on the AHe data

Table 2 Detailed apatite fission-track length data

Sample	n CT	CT mean (μm)	CT std (μm)	CT skew	Lc mean (μm)	Lc std (μm)	Lc skew	n Dpar	Dpar mean (μm)	Dpar std (μm)	Dpar skew
Northern Rwenzori Mtns											
RZ03-29	92	12.1	1.3	-0.08	13.6	1.2	-0.33	462	1.4	0.2	0.34
RZ03-33	110	10.7	1.5	-0.06	12.7	1.1	-0.57	152	1.5	0.3	1.53
Central Rwenzori Mtns											
RZ03-02	145	11.8	1.6	-0.06	13.5	1.2	-0.27	77	2.0	0.5	0.22
RZ03-03	84	11.7	1.4	0.08	13.1	1.2	-1.53	320	1.6	0.2	0.83
RZ03-04	69	12.0	1.4	-0.48	13.5	1.1	-0.70	184	1.9	0.3	1.23
RZ03-05	2	12.1	1.0	-	-	-	-	62	1.8	0.5	0.62
RZ03-07	104	11.4	1.5	-0.11	13.2	1.1	-0.60	192	1.5	0.2	0.42
RZ03-08	7	11.7	1.2	0.47	12.6	1.7	0.07	85	1.5	0.3	0.80
RZ03-09	34	11.6	1.5	-0.01	13.3	1.0	-0.39	169	1.6	0.3	0.40
RZ03-10	22	12.1	1.3	-0.77	13.7	1.1	-1.12	140	1.6	0.4	-0.12
RZ03-11	101	11.7	1.6	-0.08	13.4	1.1	-0.05	223	1.5	0.2	-0.27
RZ03-12	84	11.9	1.8	-0.57	13.5	1.2	-0.47	228	1.6	0.4	0.28
RZ03-15	199	11.7	1.7	-0.28	13.4	1.2	-0.35	331	1.9	0.2	0.06
RZ03-26	77	11.9	1.5	0.10	13.3	1.3	-0.66	338	1.8	0.4	1.58
RZ03-27	106	12.1	1.3	-0.29	13.6	1.0	-0.81	182	1.7	0.3	0.65

n CT: number of confined tracks measured; CT mean: mean confined track length, std: standard deviation, skew.: skewness of distribution relative to the mean value (measure of asymmetry of the distribution), Lc mean: mean track length after c-axis correction, n D_{par}: number of etch pit diameters measured, D_{par} mean: mean etch pit diameter

(Table 3). A positive correlation between single grain AHe ages and the eU factor is illustrated in Fig. 8. Because of its lower eU content, sample RZ03-26 was plotted separately (Fig. 8, bottom), but also displays a positive correlation.

Modelling the thermal history: t–T modelling

The confined track length and D_{par} distribution together with the AFT cooling ages of 11 samples (Table 2) were used to model their individual thermal history (Fig. 9a–e). To improve the modelling results, AHe data as well as information on the general geological evolution from the area were considered and implemented as t–T constraints. In general, the steady cooling-only solution is concordant with the FT data of the samples. Apart from two models (RZ03-29; RZ03-07), the derived modelling solutions indicate a goodness of fit (GOF) greater than 90%, both for the best fit of the generated cooling paths and the confined FT length distribution. For sample RZ03-29, the length distribution could not be reproduced better than 60% in the inverse HeFTy model, the accordant t–T path, however, fits the data set very well (GOF: 1.0). In the case of sample RZ03-07, the modelled length distribution matches the measured one with 89% confidence (GOF: 0.89), while the best fit for the t–T path reaches a value of 80%, which is still acceptable, but needs to be considered for interpretation. All models have more than 40 good t–T paths and at

least 200 accepted t–T paths; the majority, however, reveals more than 200 good and 1000 accepted t–T paths.

In general, the shape of the cooling path of all samples is characterized by initially fast cooling to about 70°C in the Mesozoic, followed by very slow cooling in Mesozoic and Palaeogene times to 50–40°C, and rapid cooling in the Neogene to surface temperature. The resulting exhumation rates over time vary between 1.333 mm/a, and 0.003 mm/a (Table 4). For calculating exhumation rates from the thermochronological data set, several assumptions need to be made. The average recent surface temperature (T_s) was set 20°C at lower elevations and 15°C at higher elevations. Regarding the geothermal gradients two distinct values were used, depending on the cooling gradient. For times of slow cooling, a general geothermal gradient of 25°C/km was assumed. In time segments with fast cooling, however, a geothermal gradient of 30°C/km was applied. In view of the geological background, it can be presumed that amplified cooling of rocks in the Rwenzori Mtns was triggered by enhanced vertical rock movements and erosion, rather than by erosion solely. Therefore, an increased geothermal gradient of 30°C/km was assumed for times of fast cooling, and 25°C/km for times of slow cooling. At present, the geothermal gradient in the Lake Albert Basin sediments increases from S (~50°C/km southern Lake Albert) to N (~70°C/km northern Lake Albert, P. Logan, personal communication). In general, increased geotherms

Table 3 Summary of apatite (U–Th–Sm)/He data

Sample	M (μg)	Av. <i>r</i> (μm)	U ($\mu\text{g/g}$)	Th ($\mu\text{g/g}$)	Sm ($\mu\text{g/g}$)	^4He (nmol/g)	eU ($\mu\text{g/g}$)	F_t	Raw age (Ma)	1σ (Ma)	Corr. age (Ma)	1σ (Ma)
Northern Rwenzori Mtns												
RZ03-32a1	3.6	49	47	<1	244	12.77	47	0.74	49.47	1.12	66.76	1.51
RZ03-32a2	1.2	34	21	1	133	4.97	21	0.64	43.25	1.21	68.10	1.90
RZ03-32a3	12.5	72	34	1	263	13.20	34	0.81	71.43	1.54	88.14	1.91
RZ03-34a1	1.0	38	20	3	114	15.19	21	0.64	134.36	3.84	209.99	6.01
RZ03-34a2	0.9	34	22	5	275	13.12	23	0.62	103.99	2.98	168.70	4.83
RZ03-34a3	2.2	54	41	4	204	25.51	42	0.73	112.28	2.44	154.39	3.36
Central Rwenzori Mtns												
RZ03-02a1	1.4	39	97	27	162	23.20	103	0.67	41.30	0.85	61.88	1.27
RZ03-02a3	2.0	48	114	16	120	26.05	118	0.71	41.05	0.81	57.75	1.14
RZ03-02a4	3.8	55	49	4	183	5.49	50	0.76	20.32	0.41	26.86	0.54
RZ03-03a1	2.4	41	7	6	167	3.61	8	0.69	74.27	1.42	107.06	2.05
RZ03-03a2	4.5	60	13	14	145	8.80	16	0.77	97.32	1.86	127.21	2.43
RZ03-04a1	4.7	65	10	4	42	3.40	11	0.78	58.74	1.20	75.45	1.54
RZ03-04a2	1.5	37	15	8	58	5.84	17	0.66	65.29	1.43	99.53	2.19
RZ03-07a1	1.3	33	20	43	95	12.06	30	0.62	74.43	1.31	120.40	2.11
RZ03-07a2	2.6	48	15	28	50	8.70	22	0.71	75.18	1.33	105.28	1.86
RZ03-08a1	1.1	31	11	20	88	6.71	16	0.60	79.38	1.53	132.86	2.56
RZ03-08a2	0.9	31	16	24	70	5.39	22	0.59	45.90	0.86	77.23	1.45
RZ03-09a1	1.1	33	7	24	76	4.83	13	0.61	67.44	1.22	110.93	2.01
RZ03-09a2	1.0	37	9	25	41	4.78	15	0.63	60.93	1.10	97.11	1.75
RZ03-10a1	1.7	33	15	26	121	5.78	21	0.63	50.99	0.93	80.87	1.48
RZ03-10a2	2.5	46	5	28	108	1.08	12	0.70	17.37	0.33	24.91	0.47
RZ03-12a1	2.8	49	11	28	60	6.14	18	0.72	63.71	1.10	88.88	1.54
RZ03-12a2	5.9	65	14	38	57	7.37	23	0.78	59.10	1.01	75.89	1.30
RZ03-16a1	1.2	27	21	1	45	5.29	21	0.58	46.58	1.01	80.24	1.74
RZ03-16a2	3.1	42	12	1	41	3.00	12	0.71	47.17	1.03	66.49	1.45
RZ03-26a1	2.0	38	6	8	441	1.20	8	0.67	25.71	0.49	38.46	0.73
RZ03-26a2	2.0	39	7	16	347	3.78	12	0.67	59.73	1.08	89.20	1.61
RZ03-26a3	3.8	50	6	15	321	4.07	10	0.73	74.32	1.34	101.44	1.83
RZ03-26a4	4.4	52	6	10	325	1.56	8	0.75	33.96	0.66	45.55	0.89
RZ03-26a5	26.7	94	7	11	411	3.03	10	0.85	57.42	0.94	67.19	1.10
RZ03-26a6	9.0	70	7	11	410	1.48	10	0.80	27.75	0.47	34.60	0.58
RZ03-27a1	26.0	93	22	6	45	8.62	23	0.86	67.70	1.39	78.92	1.62
RZ03-27a2	1.2	33	31	14	88	10.02	34	0.63	53.93	1.09	85.96	1.73
RZ03-27a3	1.0	33	9	15	37	2.82	13	0.61	40.10	1.31	66.16	2.16
RZ03-27a4	1.4	35	55	31	161	23.63	62	0.64	70.07	1.34	108.93	2.08
RZ03-27a5	3.0	43	91	31	148	35.74	98	0.71	66.66	1.28	93.89	1.80
RZ03-27a6	3.1	53	11	7	38	2.74	13	0.74	39.16	0.80	52.94	1.09

a1–a6 analysed apatite grain; *M* mass; Av. *r* average radius, derived from two width measurements; contributing U-, Th-, and Sm-, and ^4He concentration; eU = [U] + 0.235[Th] (concentrations in weight %); F_t : α -ejection correction factor calculated according to Farley model (Reiners and Farley 2001); raw AHe ages and 1σ -error are corrected (corr.) for alpha ejection with accordant 1σ -error. Elevation, latitude, longitude, and lithological description see Table 1

in the rift valleys of the EARS are thought to be due to current geothermal activity (e.g. D'Oreye et al. 2007). The applied geothermal gradients are average gradients for a long time span of millions of years. The onset of recent high heat flow is not known. As shown by Nyblade (1997)

and Nyblade et al. (1990), such heat flow values cannot be directly transferred to neighbouring cratonic areas. Geothermal gradients between 25 and 30°C/km, therefore, seem reasonable estimates for rift flanks and cratonic areas in the EARS and are in accordance with other studies in

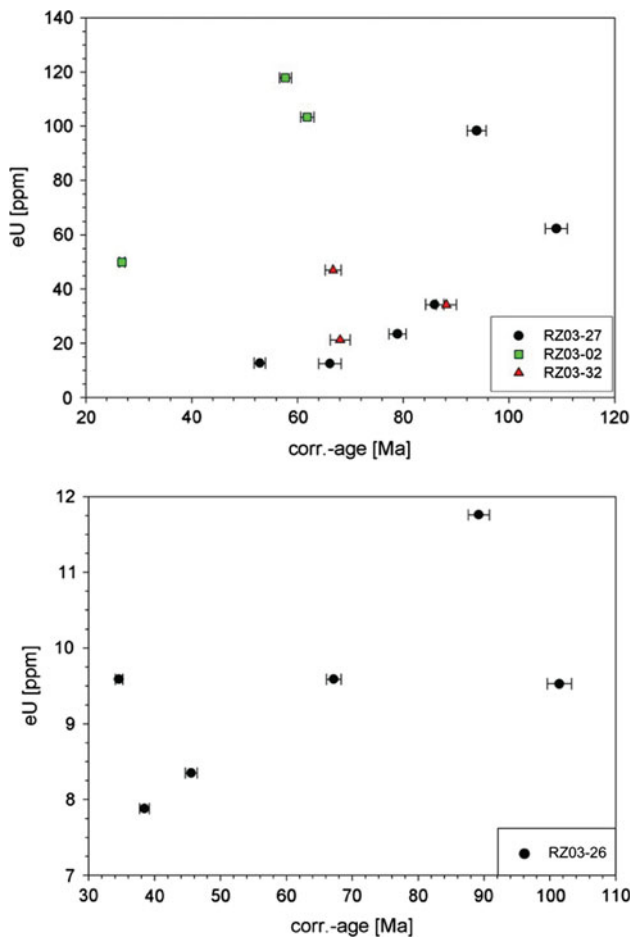


Fig. 8 Dependency of AHe ages on the eU-factor (see Text for further detail)

this tectonic setting (e.g. van der Beek et al. 1997; Abbate et al. 2002; Spiegel et al. 2007).

Interpretation of AFT and AHe ages

The AFT and AHe ages and track length distributions indicate a very complex cooling history that affected the Rwenzori Mtns since at least the Mesozoic. The data set matches structural observations from the Rwenzori Mtns pointing to different generations of fault sets, overprinting each other (cp. Ring 2008). They, furthermore, fit into the common age pattern shown by other thermochronological studies of the EARS (e.g. van der Beek et al. 1998; Spiegel et al. 2007), and are in general accordance with the data by MacPhee (2006). The data set of MacPhee is characterized by a wide spread in AHe ages [262.5 (± 6.39) Ma to 18.9 (± 0.5) Ma; elevations: 690 m to 4,620 m a.s.l.], whereas no age elevation relationship was observed. This matches the results gained by the authors of this contribution, with AHe ages of 210.0 (± 6.0) Ma to 24.9 (± 0.5) Ma also lacking any age elevation relationship.

As described earlier, several factors influence the diffusion behaviour and accumulation of He and may account for large spreads in single grain AHe ages. In this study, no relationship between AHe ages and variable grain size as described by Reiners and Farley (2001) could be observed. Another possible cause for variations of AHe ages is the injection of α -particles. Some of the analysed samples contain a considerable amount of U- and Th bearing minerals such as zircon, which is also displayed by a raised U- and Th concentration (>20 ppm; e.g. RZ03-02, RZ03-4; RZ03-16; RZ03-23) (Nagudi et al., in preparation). Therefore, the possible influence of α -particle injection should be considered. High U-, and Th concentrations, in combination with a prolonged cooling history, furthermore, might increase the accumulation of radiation damage in the crystal lattice (Fitzgerald et al. 2006; Flowers et al. 2006, 2009). Within errors, four of the analysed samples indicate a positive correlation with the eU factor (Table 3; Fig. 8), pointing to such an increase of crystal defects due to radioactive decay (Shuster et al. 2006; Shuster and Farley 2009). To better evaluate corresponding effects on the AHe ages in the Rwenzori Mtns, more apatite grains need to be analysed. Despite these irritating factors, the AHe ages reveal valuable information on the timing of movement through the $\sim 70^\circ\text{C}$ isotherm. Both radiation damage and α -injection will lead to AHe ages that will be older than the age of an unaffected apatite crystal. Only very young AHe ages that are not reproduced by other samples should be excluded, as they might reflect enhanced He loss due to fire (cp. Mitchell and Reiners 2003). As this was not the case for the presented data set, the youngest AHe ages are considered to provide the most reliable estimate of the cooling below $\sim 70^\circ\text{C}$. A similar approach for slowly cooled terrains was suggested by Fitzgerald et al. (2006), considering a cooling age between the minimum age and the weighted mean age as the most representative. However, having for some samples just two single grain ages, we refer to the youngest AHe ages as the most representative. Following this approach, young cooling ages (AHe) occurring on different elevations such as 24.9 (± 0.5) Ma at 4,150 m a.s.l., 26.9 (± 0.5) Ma at 1,900 m a.s.l., and 34.6 (± 0.6) Ma at 1,690 m a.s.l. point to a very young and fast exhumation of the Rwenzori Mtns, with cooling below $\sim 70^\circ\text{C}$ in Oligocene time.

Discussion

Ages versus faults

The AFT age distribution ranges from 85.3 (± 5.3) Ma to 195.0 (± 8.4) Ma, with the majority of samples from the central part scattering around 130 Ma. No age elevation relationship can be derived. Major variations in cooling

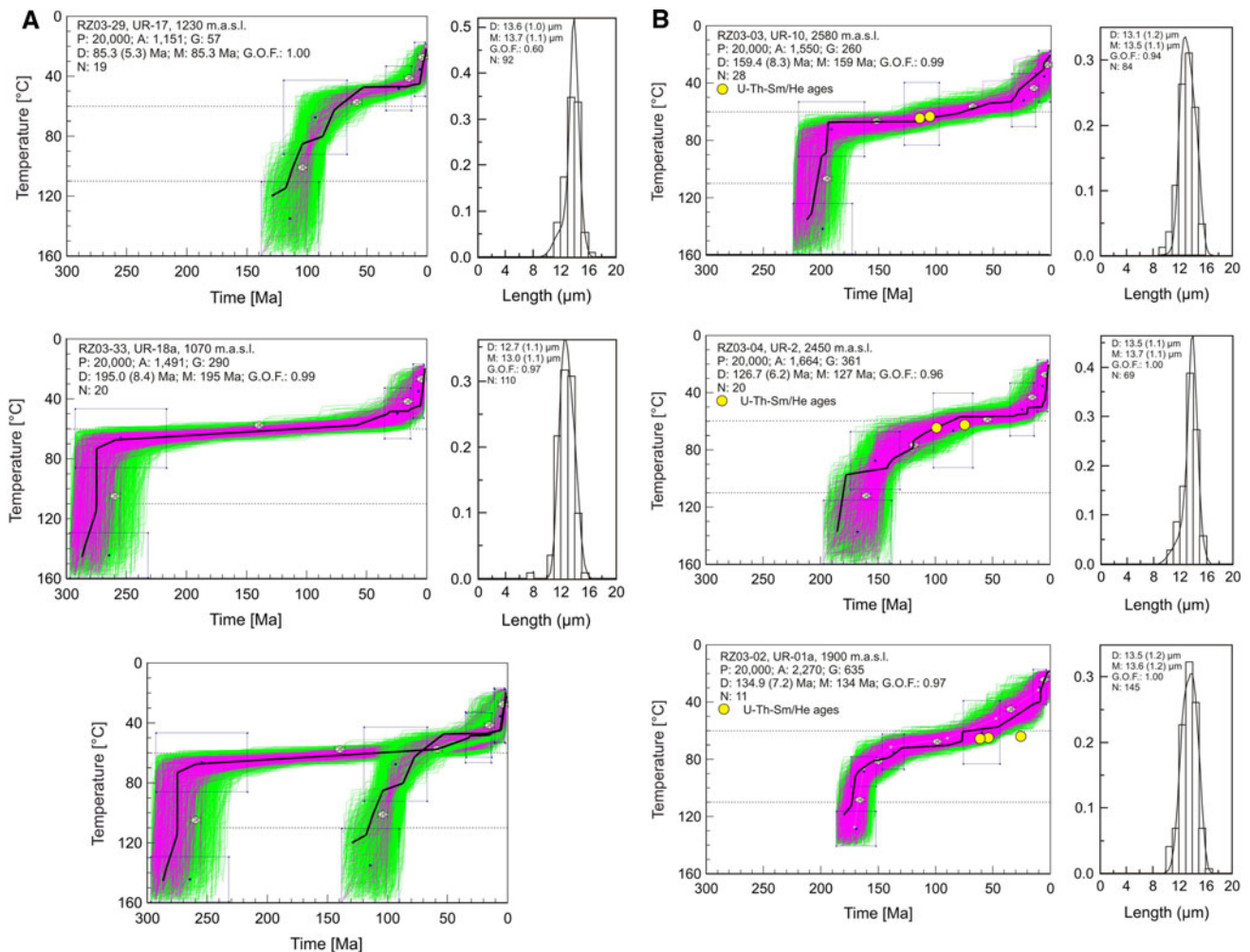


Fig. 9 a–e Results from thermal modelling (HeFTy, Ketcham et al. 2009), with revealed t - T paths illustrating the cooling history of individual samples from the northern part (**a**), and across the central Rwenzori Mtns (**b–d**). Displayed are the t - T paths (*left*), and the c -axes corrected confined fission-track length (CT) frequency distribution (*right*) overlain by a calculated probability density function (*best fit*). The modelling tests possible t - T curves that fit independent geological constraints (*squares*) against the AFT data set. The results in the t - T curve show three different reliability levels; green paths: acceptable fit = all t - T paths with a merit function value of at least 0.05, pink paths: good fit = all t - T paths with a merit function value of at least 0.5, black line: best fit (Ketcham et al. 1999, 2009). P : number of tested inverse models, A acceptable fit models, G good fit models, D determined FT age ($1-\sigma$ error) and CT, M modelled FT age, and CT, $G.O.F.$ goodness of fit, N number of single grains and measured CT. AHe ages are not modelled because of their probable eU dependence, but used as geological constraints and plotted along

t - T paths, where available. Please see text for explanation of the modelled samples. **a** t - T paths of samples RZ03-29 (*top*), and RZ03-33 (*middle*), northern Rwenzori Mtns; *bottom* t - T paths of both samples, illustrating their different thermal evolution. Sample RZ03-33 passed the PAZ much earlier (~ 280 Ma) than sample RZ03-29 (~ 115 – 50 Ma), after ~ 50 Ma both samples had a similar cooling history. **b** t - T paths of samples RZ03-03, RZ03-04, and RZ03-02, central Rwenzori Mtns, with similar cooling paths. **c** t - T paths of samples RZ03-11, and RZ03-07, central Rwenzori Mtns, with similar cooling paths. **d** t - T paths of samples RZ03-27 (*top*), and RZ03-26, central Rwenzori Mtns, taken from both sides of fault A (Fig. 2); *bottom*: t - T paths of both samples, illustrating their different exhumation history before ~ 90 Ma (see text for further explanations). **e** t - T paths of samples RZ03-12 (*top*), and RZ03-15 (*middle*), central Rwenzori Mtns, taken from both sides of a valley; t - T paths of both samples (*bottom*), illustrating a similar t - T evolution after 195 Ma (see text for further explanations)

ages revealed by AFT analysis are related to movements along normal faults as discussed in the following (Figs. 2, 7).

The AFT ages from the northern part of the Rwenzori Mtns [195.0 (± 8.4) Ma at eastern flank and 85.3 (± 5.3) Ma at western flank] indicate movements at the eastern flank as early as 195 Ma ago, and at the western flank ~ 85 Ma ago. This might point to pre-existing faulting along the

Rwimi-Wasa and Bwamba faults, presently delimiting the mountain range (Fig. 2). The modelled t - T paths of samples RZ03-33 and RZ03-29 from the northern Rwenzori Mtns suggest that these samples had distinctly different thermal evolutions at temperatures $>60^\circ\text{C}$ (Fig. 9a). At about 30 Ma and 50°C , both samples evolve in a similar way. Sample RZ03-33 (1,070 m a.s.l.) with the oldest AFT

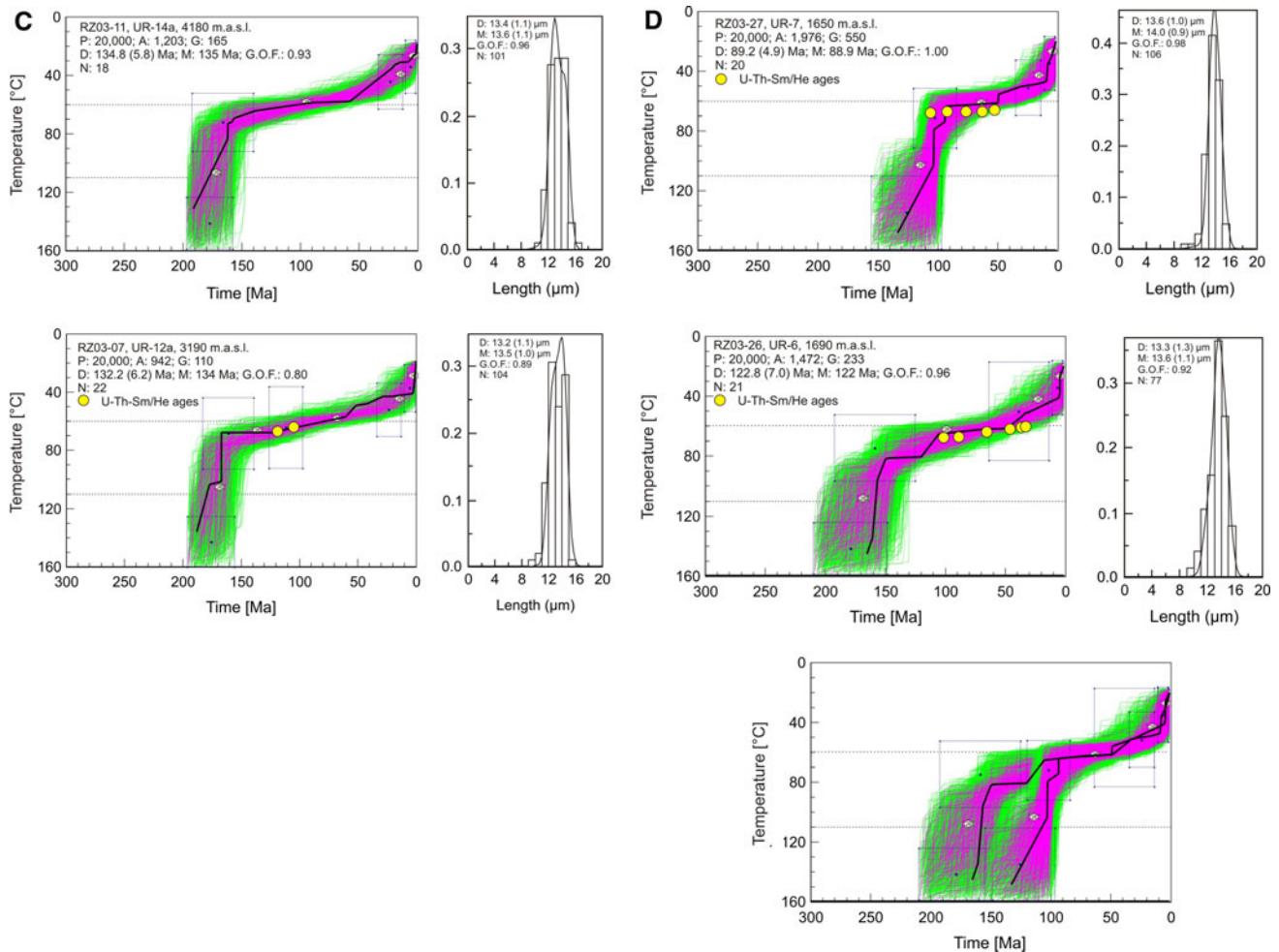


Fig. 9 continued

age ($195.0 (\pm 8.4)$ Ma) cooled rapidly below 110°C at about 280 Ma and reached 70°C shortly after. This rapid cooling was followed by prolonged very slow cooling between 280 Ma and 30 Ma to about 50°C . The younger sample (RZ03-29, 1,230 m a.s.l.; $85.3 (\pm 5.3)$ Ma) cooled from 110°C to 50°C between 115 Ma and 50 Ma. Thereafter, the samples had a similar cooling history with a cooling rate of $5^{\circ}\text{C}/\text{Ma}$ (Table 4) showing no difference in cooling in the footwalls of the Bwamba and Rwimi-Wasa faults.

In the central Rwenzori Mtns, the majority of AFT ages is similar (~ 130 Ma), despite differences in elevation of more than 3,000 m (1,690 m a.s.l. to 4,800 m a.s.l.). Correspondingly, their cooling paths are also similar (Fig. 9b, c). Fast cooling from 110°C to 80°C occurred between 175 and 165 Ma, where a topography of about 1,500 m could have been created if surface uplift exceeded the erosion rate. This phase is followed by slow cooling to about 40°C at ~ 5 Ma. Final cooling to surface temperature is rapid

again. Initial exhumation rates were ~ 0.1 mm/a and slowed down to about 0.005 mm/a (Table 4). Since the Neogene, exhumation rates were of the order of 0.133–0.200 mm/a (Table 4).

Two exceptions regarding the AFT ages have been encountered along the central transect. One is related to movements along a \sim NNW–SSE trending fault (indicated A in Fig. 2). Samples taken from both sides of the fault revealed a significant age difference of 30 Ma. Sample RZ03-27 with $89.2 (\pm 4.9)$ Ma was taken E of fault A at an elevation of 1,650 m a.s.l., and sample RZ03-26 with $122.8 (\pm 7.0)$ Ma was taken W of the fault at an elevation of 1,690 m a.s.l. Thus, at about 90 Ma, sample RZ03-27 moved into the partial annealing zone, indicating activity along the fault that might have led to a displacement of about 1.6 km for a thermal gradient of $25^{\circ}\text{C}/\text{km}$ (1.4 km for $30^{\circ}\text{C}/\text{km}$). After 90 Ma, both sides have exhumed in a similar way as indicated by the cooling paths (Fig. 9d). For interpretation of corresponding AHe ages, the individuality

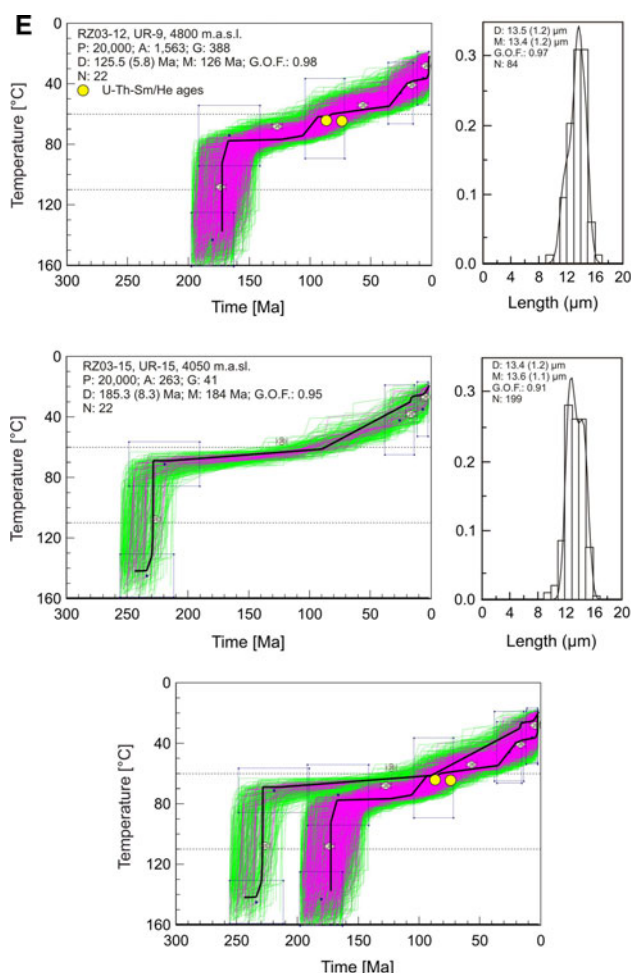


Fig. 9 continued

of each apatite grain needs to be considered. As indicated by Fig. 8, the AHe ages correlate with the eU factor. This indicates that the increase of dislocations caused by α -particles during radioactive decay changed the diffusion kinetics within every grain individually and might account for the spread in AHe ages. It further suggests that both blocks remained within the partial retention zone for long time, enhancing the various kinetics effects.

The second exception was encountered along a deep NW–SE trending valley near the high peaks of the Rwenzori Mtns. Samples RZ03-12 (125.5 (\pm 5.8) Ma) and RZ03-15, (185.3 (\pm 8.3) Ma) from both sides of the valley show differences in elevation of \sim 750 m and differences in AFT ages of \sim 60 Ma (Fig. 7). Whereas the lower sample (RZ03-15) at 4,050 m a.s.l. revealed the oldest AFT age along the transect so far. As indicated by their cooling paths (Fig. 9e) both samples experienced similar t–T conditions after 170 Ma. As described earlier, different fault sets that are overprinting each other can be observed in the Rwenzori Mtns and often can be traced by

correspondingly trending valleys (Ring 2008, Bauer et al., *in review*). Most likely the detected age variation is related to an old fault (indicated B in Fig. 2) that follows the direction of the valley and was active at \sim 170 Ma.

Periods of accelerated cooling and comparison with other parts of the EARS

A first phase of accelerated cooling below 110°C affected the north-eastern area of the Rwenzoris at about 280 Ma, whereas \sim 70°C were reached locally shortly after. A second phase of accelerated cooling below 110–80°C was recorded between 175 and 165 Ma for most samples of the central Rwenzori Mtns. These episodes of cooling roughly coincide with previous studies, e.g., by van der Beek et al. (1998), Foster and Gleadow (1992, 1993), reporting early denudation events at around 250–200 Ma and 150–120 Ma. As proposed by Foster and Gleadow (1993), such regional phases of denudation can be correlated to processes of tectonic reorganization and intracontinental deformation. The first accelerated cooling phase at about 280 Ma might be related to movements that affected the area during the consolidation of Pangaea. A slightly younger cooling event (\sim 250 Ma) shown by van der Beek et al. (1998) is interpreted as major erosional event at the end of the Karoo sedimentary regime. Very few occurrences of Karoo in Uganda and the Western Rift as well as reports about Karoo sediments of the Ecca Group underlying Miocene rift sediment (Schlueter 1994) suggest that this erosional event might have also affected the Albertine Rift. As discussed by Torsvik et al. (2008), absolute plate motions of the Gondwana realm changed in time, from northeast (250 Ma) through southwest (180 Ma) to southward motion (170 Ma) until the end of the Jurassic. We propose that effects of these reconfigurations are detectable in the thermochronological data set from the Rwenzori Mtns. The tectonic movements at \sim 190 and 170 Ma and cooling at about 175 Ma roughly coincide with cooling episodes described from Madagascar (Emmel et al. 2008), pointing to plate motions that finally lead to the breakup of Gondwana and the onset of rifting between East Africa and Madagascar.

A third accelerated cooling episode from 110°C to 50°C occurred between 115 and 50 Ma, which is contemporaneous with the rift and drift phase of the South Atlantic (e.g. Bumby and Guiraud 2005), was observed only locally. Upper Cretaceous to Palaeocene (70–40 Ma) cooling events were also reported e.g. by van der Beek et al. (1998), Foster and Gleadow (1992, 1993) and Spiegel et al. (2007) and are correlated with major plate reorganisation in the Indian Ocean. Throughout the Late Palaeozoic, Mesozoic and Cenozoic era, the East African realm seems to be affected by distinct phases of surface uplift and erosion,

Table 4 Main t–T segments and exhumation rates of the northern and central Rwenzori Mtns

Sample	Elevation (m a.s.l.)	Cooling	t-t segment (Ma)	T-T segment (°C)	Cooling gradient (°C/Ma)	Geothermal gradient (°C/km)	Exhumation rate (mm/a)
Northern Rwenzori Mtns							
RZ03-29	1230	Fast	115–50	110–50	0.92	30	0.031
RZ03-29	1230	Very slow	50–5	50–45	0.11	25	0.004
RZ03-29	1230	Very fast	5–recent	45–20	5.00	30	0.167
RZ03-33	1070	Very fast	280–275	110–70	8.00	30	0.267
RZ03-33	1070	Very slow	275–30	70–50	0.08	25	0.003
RZ03-33	1070	Very slow	30–5	50–45	0.20	25	0.008
RZ03-33	1070	Very fast	5–recent	45–20	5.00	30	0.167
Central Rwenzori Mtns							
RZ03-03	2580	Very fast	205–195	110–70	4.00	30	0.133
RZ03-03	2580	Slow	195–30	70–50	0.12	25	0.005
RZ03-03	2580	Fast	30–recent	50–15	1.17	30	0.039
RZ03-15	4050	Very fast	231–230	110–70	40.00	30	1.333
RZ03-15	4050	Slow	230–90	70–60	0.07	25	0.003
RZ03-15	4050	Slow	90–recent	60–15	0.50	25	0.020
RZ03-26	1690	Very fast	160–150	110–80	3.00	30	0.100
RZ03-26	1690	Fast	150–105	80–65	0.33	30	0.011
RZ03-26	1690	Slow	105–50	65–60	0.09	25	0.004
RZ03-26	1690	Fast	50–5	60–40	0.44	30	0.015
RZ03-26	1690	Very fast	5–recent	40–20	4.00	30	0.133
RZ03-27	1650	Very fast	110–90	110–65	2.25	30	0.075
RZ03-27	1650	Slow	90–50	65–60	0.13	25	0.005
RZ03-27	1650	Fast	50–5	60–40	0.44	30	0.015
RZ03-27	1650	Very fast	5–recent	40–20	4.00	30	0.133
RZ03-12	4800	Very fast	175–165	110–80	3.00	30	0.100
RZ03-12	4800	Slow	165–20	80–45	0.24	25	0.010
RZ03-12	4800	Slow	20–3	45–35	0.59	25	0.024
RZ03-12	4800	Very fast	3–recent	35–15	6.67	30	0.222
RZ03-11	4180	Fast	180–160	110–70	2.00	30	0.067
RZ03-11	4180	Slow	160–20	70–35	0.25	25	0.010
RZ03-11	4180	Slow	20–5	35–30	0.33	25	0.013
RZ03-11	4180	Very fast	5–recent	30–15	3.00	30	0.100
RZ03-07	3190	Very fast	180–165	110–70	2.67	30	0.089
RZ03-07	3190	Slow	165–3	70–40	0.19	25	0.007
RZ03-07	3190	Very fast	3–recent	40–15	8.33	30	0.278
RZ03-04	2450	Very fast	180–175	110–100	2.00	30	0.067
RZ03-04	2450	Fast	175–80	100–60	0.42	30	0.014
RZ03-04	2450	Slow	80–5	60–50	0.13	25	0.005
RZ03-04	2450	Very fast	5–recent	50–20	6.00	30	0.200
RZ03-02	1900	Very fast	175–170	110–90	4.00	30	0.133
RZ03-02	1900	Slow	170–130	90–70	0.50	25	0.020
RZ03-02	1900	Slow	130–10	70–40	0.25	25	0.010
RZ03-02	1900	Very fast	10–recent	40–20	2.00	30	0.067

Exhumation rates were calculated considering cooling rate, surface temperature and thermal gradient. Depending on the cooling pattern of the modelled t–T paths a geothermal gradient of either 25°C/km (slow cooling) or 30°C/km (fast cooling) was applied (see text for further explanations)

with no major heating event affecting the area in respect of affecting the low-temperature thermochronometric clock. Plume activities, as discussed, e.g., for South Africa (~ 182 Ma Karoo volcanics; ~ 135 Ma Parana-Etendeka volcanic rocks) and the Afar region (~ 31 Ma) (cp. Torsvik et al. 2008; Bumby and Guiraud 2005, Ebinger and Sleep 1998) are regarded as driving forces, allowing for surface uplift by doming and subsequent erosion of the area. An increased heat flow, affecting the upper crust and accordant isotherms of the AFT and AHe system of the entire Western Rift can be excluded (cp. heat flow studies by Nyblade 1997).

The last major cooling episode at about 30 Ma is similar for most samples of the Rwenzori Mtns and is detected by other thermochronological studies as well (Fig. 6). Thermal modelling of the samples from the Rwenzori Mtns reveals accelerated cooling with an onset at ~ 30 Ma with a differential cooling history (Fig. 9). The Neogene cooling episode, also observed e.g. by van der Beek et al. (1998) for the Rukwa-Malawi sector of the western branch, is related to movements within the EARS and reflects surface uplift due to doming with subsequent rift initiation and erosion (Fig. 3) (Ebinger 1989; Ebinger and Sleep 1998). The differential cooling history displays distinct phases of exhumation (rock uplift and erosion) that affected the Rwenzori Mtns. During the initial stage of Neogene surface uplift lithological units (possible Karoo series and metamorphic rocks) overlying the recent surface were eroded, resulting in AHe ages of ~ 25 Ma. As confirmed by these cooling ages, the final uplift that partly led to the formation of the recent topography must have been fast and probably started a few ka to Ma ago. Possible mechanisms allowing for this uplift are discussed by Koehn et al. (2010) and Wallner and Schmelting (2010) in this issue. We assume that the erosion rate did not compensate the rock uplift rate leading to the recent high topography. This is consistent with observations obtained from clay minerals of brittle faults (fault gouge samples) that were not yet sufficiently exhumed (Haines 2008) to reveal clay minerals formed at higher temperatures. Long-term or strong erosion of the metamorphic basement would have caused either a positive or a negative slope of the regression line in an age-elevation diagram (Braun 2002). The very rapid final cooling to surface temperatures in Pliocene to Pleistocene times can also be derived from the individual t - T paths of the thermal models. This corroborates the hypothesis, stated e.g. by Pickford et al. (1993) that major surface uplift of the Rwenzori Mtns occurred after ~ 2.5 Ma, splitting Lake Obweruka into Lake Edward and Lake Albert.

The different phases of Neogene exhumation are also reflected by the morphology and landscape of the Rwenzori Mtns and surrounding areas (Figs. 4, 5). The rugged high

mountain ranges and associated levels of erosion reveal a differentiated topography with marked phases of surface and rock uplift, while the steep western flank point to more pronounced movements along the Bwamba border faults at the western flank. AFT and AHe ages indicate that since the formation of the high topography the erosion rate was too low to expose rocks with younger cooling ages.

Conclusion

From thermal modelling, which considers AFT ages, CT length distribution, D_{par} as well as further geological constraints, a protracted cooling history can be derived for the Rwenzori Mtns, with integrated episodes of major cooling. Determined cooling ages as well as cooling patterns are in accordance with the thermochronological studies known from the EARS and may coincide with phases of plate reconfiguration, related to the consolidation of Pangaea and following breakup of Gondwana.

The Permo-Triassic cooling phase observed in the Rwenzori Mtns might reveal movements that affected the area during the consolidation of Pangaea and a subsequent major erosional event at the end of the Karoo sedimentary regime.

In Middle to Upper Jurassic, the area was affected by fast exhumation. This might have led to an area with minor topography if the erosion compensated for the fast rock uplift. However, if the rock uplift exceeded the erosion rate, this might lead to a surface uplift causing an elevation of up to 1,500 m a.s.l.

This phase was followed by slow constant cooling during most of Cretaceous and Palaeogene times, where very minor rock uplift might have been compensated by the erosion rate. Movements along faults differentiated the topography in the late Cretaceous. If the erosion rate was low differential topography might have been initiated by a higher surface uplift rate.

Accelerated cooling affected the Rwenzori Mtns again in Neogene times. During the initial stage of the Neogene rock uplift erosion rates of more than 0.2 mm/a exhumed the sampled rocks near to the surface and might have accounted for a low relief.

The final surface uplift of the central Rwenzori Mtns that partly led to the formation of the recent topography must have been fast and in the near past (Pliocene to Pleistocene). Erosion could not compensate for the rock uplift, resulting in the recent high topography and Oligocene to Miocene AHe ages.

Acknowledgments We thank the *RiftLink* research group and our partners from Makerere University for discussion on the Rwenzori geology as well as for the support in the field. We also thank the Uganda National Council for Science and Technology (UNCST) as

well as the Uganda Wildlife Authority (UWA) for supporting field-work. Furthermore, we would like to thank Peter W. Reiners and Stefan Nicolescu for analytical assistance and valuable discussions. Matthias Hinderer and Martin Wipf are thanked for their constructive suggestions and comments on an earlier version of the manuscript. For providing the computer code HeFTy we would like to express our thanks to Richard A. Ketcham and Raymond A. Donelick, and to Raymond A. Donelick, allowing using D_{par} as a kinetic parameter. ASTER GDEM, product of METI & NASA is thanked for providing their images. We furthermore appreciate the support given by Heiko Gerstenberg and the Forschungs-Neutronenquelle FRM II at Garching, TU München. Acknowledgement is given to the German Research Foundation (Deutsche Forschungsgemeinschaft, DFG) for their support (GL 182/9-1) and for funding the project (DFG research unit 703). The University Mainz is gratefully acknowledged for a grant supporting a pilot study.

References

- Abbate E, Balestrieri ML, Bigazzi G (2002) Morphostructural development of the Eritrean rift flank (southern Red Sea) inferred from apatite fission track analysis. *J Geophys Res* 107:2319–2331
- Abeinomuqisha D, Mugisha F (2004) Structural analysis of the Albertine graben, Western Uganda. Abstract, East African rift System Evolution, Resources and Environmental Conference, Addis Abeba, June 2004
- Ahnert F (2003) Einführung in die Geomorphologie. Ulmer, Stuttgart
- Bahat D, Mohr P (1987) Horst faulting in continental rifts. *Tectonophysics* 141:61–73
- Batt GE, Brandon MT (2002) Lateral thinking: 2-D interpretation of thermochronology in convergent orogenic settings. *Tectonophysics* 349(1–4):185–201
- Bauer FU, Karl M, Glasmacher UA, Nagudi B, Andreas S, Mroszewski L (in review) The Rwenzori Mountains of western Uganda—an approach to unravel the evolution of a remarkable morphological feature within the Albertine Rift. Submitted to *J Afr Earth Sci*
- Bishop P (2007) Long-term landscape evolution: linking tectonics and surface processes. *Earth Surf Proc Land* 32:329–365
- Boven A, Pasteels P, Punzalan LE, Yamba TK, Musisi JH (1998) Quaternary perpotassic magmatism in Uganda (Tore-Ankole Volcanic Province): age assessment and significance for magmatic evolution along the East African Rift. *J Afr Earth Sci* 26(3):463–476
- Braun J (2002) Quantifying the effect of recent relief changes on age-elevation relationships. *Earth Planet Sci Lett* 200:331–343
- Bumby AJ, Guiraud R (2005) The geodynamic setting of the Phanerozoic basins of Africa. *J Afr Earth Sci* 43(1–3):1–12
- Davis W (1899) The geographical cycle. *Geogr J* 14:481–504
- Delvaux D, Barth A (2010) African Stress Pattern from formal inversion of focal mechanism data. Implications for rifting dynamics. *Tectonophysics* 482:105–128
- Dodson MH (1973) Closure temperature in cooling geochronological and petrological systems. *Contrib Mineral Petrol* 40:259–274
- Donelick RA, Ketcham RA, Carlson WD (1999) Variability of apatite fission-track annealing kinetics II: crystallographic orientation effects. *Am Mineral* 84:1224–1234
- D'Oreye N, Cayol V, Kervyn F, GVO (2007) The November 2006 Nyamulagira eruption revealed by InSAR. Proceeding of the 26th ECGS workshop, AVCOR07, Luxembourg, November 2007
- Donelick RA, O'Sullivan PB, Ketcham RA (2005) Apatite fission-track analysis. *Rev Mineral Geochem* 58:49–94
- Dunkl I (2002) Trackkey: a Windows program for calculation and graphical presentation of fission track data. *Comput Geosci* 28:3–12
- Ebinger CJ (1989) Tectonic development of the western branch of the East African rift system. *Geol Soc Am Bull* 101:885–903
- Ebinger CJ, Furman T (2002) Geodynamical setting of the Virunga Volcanic Province, East Africa. *Acta Vulcanol* 14(1–2):1–8
- Ebinger CJ, Sleep NH (1998) Cenozoic magmatism throughout East Africa resulting from impact of a single plume. *Nature* 395:788–791
- Ebinger CJ, Deino AL, Tesha AL, Becker T, Ring U (1993) Tectonic controls on rift basin morphology: evolution of the Northern Malawi (Nyasa) Rift. *J Geophys Res* 98(B10):17,821–17,836
- Emmel B, Jöns N, Kroener A, Jacobs J, Wartho J-A, Schenk V, Razakamanana T, Austegard A (2008) From closure of the Mozambique ocean to Gondwana breakup: new evidence from geochronological data of the Vohibory terrane, Southwest Madagascar. *J Geol* 116(1):21–38
- England P, Molnar P (1990) Surface uplift, uplift of rocks, and exhumation of rocks. *Geology* 18:1173–1177
- Farley KA (2000) Helium diffusion from apatite: general behaviour as illustrated by Durango fluorapatite. *J Geophys Res* 105(B2):2903–2914
- Farley KA, Wolf RA, Silver LT (1996) The effects of long-alpha-stopping distances on (U-Th)/He ages. *Geochim Cosmochim Acta* 60:4223–4229
- Fitzgerald PG, Baldwin SL, Webb LE, O'Sullivan PB (2006) Interpretation of (U-Th)/He single grain ages from slowly cooled crustal terranes: a case study from the Transantarctic Mountains of southern Victoria Land. *Chem Geol* 225(1–2):91–120
- Flowers RM, Bowring SA, Reiners PW (2006) Low long-term erosion rates and extreme continental stability documented by ancient (U-Th)/He dates. *Geology* 34:925–928
- Flowers RM, Ketcham RA, Shuster DL, Farley KA (2009) Apatite (U-Th)/He thermochronometry using a radiation damage accumulation and annealing model. *Geochim Cosmochim Acta* 73(8):2347–2365. doi:10.1016/j.gca.2009.01.015
- Foster DA, Gleadow AJW (1992) The morphotectonic evolution of rift-margin mountains in central Kenya: constraints from apatite fission-track thermochronology. *Earth Planet Sci Lett* 113:157–171
- Foster DA, Gleadow AJW (1993) Episodic denudation in East Africa: a legacy of intracontinental tectonism. *Geophys Res Lett* 20(21):2395–2398
- Foster DA, Gleadow AJW (1996) Structural framework and denudation history of the flanks of the Kenya and Anza Rifts, East Africa. *Tectonics* 15:258–271
- Galbraith RF (1981) On statistical models for fission track counts. *Math Geol* 13(6):471–478
- Green PF (1981) 'Track-in track' length measurements in annealed apatites. *Nucl Tracks* 5:121–128
- Green PF (1988) The relationship between track shortening and fission track age reduction in apatite: combined influences of inherent instability, annealing anisotropy, length bias and system calibration. *Earth Planet Sci Lett* 89(3–4):335–352
- Green PF, Durrani SA (1977) Annealing studies of tracks in crystals. *Nucl Track Detect* 1:33–39
- Grist AM, Ravenhurst CE (1992a). Mineral separation techniques used at Dalhousie University. In: Zentilli M, Reynolds PH (eds), Short course handbook on low temperature thermochronology, 1992. Mineral Associ Can Short Course Handb 20 Appendix 2: 203–209
- Grist AM, Ravenhurst CE (1992b). A step-by-step laboratory guide to fission track thermochronology at Dalhousie University. In: Zentilli M, Reynolds PH (eds), Short course handbook on low

- temperature thermochronology, 1992. Mineral Associ Can Short Course Handb 20 Append 1:190–201
- Haines S (2008) Transformations in clay-rich fault rocks: constraining fault zone processes and the kinematic evolution of regions. Master Thesis, University of Michigan
- Hurford AJ (1990) Standardization of fission track dating calibration: recommendation by the fission track working group of the I.U.G.S. Subcommittee on geochronology. *Chem Geol* 80:171–178
- Hurford AJ, Green PF (1982) A user's guide to fission-track dating calibration. *Earth Planet Sci Lett* 59:343–354
- Hurford AJ, Green PF (1983) The Zeta age calibration of fission-track dating. *Isot Geosci* 1:285–317
- Kampunzu AB, Bonhomme MG, Kanika M (1998) Geochronology of volcanic rocks and evolution of the Cenozoic Western Branch of the East African Rift System. *J Afr Earth Sci* 26(3):441–461
- Karner GD, Byamungu BR, Ebinger CJ, Kampunzu AB, Mukasa RK, Nyakaana J, Rubondo ENT, Upcott NM (2000) Distribution of crustal extension and regional basin architecture of the Albertine rift system, East Africa. *Mar Petrol Geol* 17:1131–1150
- Ketcham RA (2005) Forward and inverse modelling of low-temperature thermochronometry data. In: Reiners PW, Ehlers TA (eds), *Low-temperature thermochronology: techniques, interpretations and applications*. *Rev Mineral Geochem* 58:275–314
- Ketcham (2009) HeFTy version 1.6.7, Manual
- Ketcham RA, Donelick RA, Carlson WD (1999) Variability of apatite fission-track annealing kinetics: III. Extrapolation to geological time scales. *Ame Mineral* 84:1235–1255
- Ketcham RA, Carter A, Donelick RA, Barbarand J, Hurford AJ (2007a) Improved measurements of fission-track annealing in apatite. *Ame Mineral* 92:789–798
- Ketcham RA, Carter A, Donelick RA, Barbarand J, Hurford AJ (2007b) Improved modeling of fission-track annealing in apatite. *Ame Mineral* 92:799–810
- Ketcham RA, Donelick RA, Balestrieri ML, Zattin M (2009) Reproducibility of apatite fission-track length data and thermal history reconstruction. *Earth Planet Sci Lett* 284:504–515
- Koehn D, Aanyu K, Haines S, Sachau T (2008) Rift nucleation, rift propagation and the creation of basement micro-plates within active rifts. *Tectonophysics* 458:105–116
- Koehn D, Lindenfeld M, Rumpker G, Aanyu, Haines S, Passchier C (2010) Active transection faults in rift transfer zones: Evidence for rotating stress fields in the East African Rift and implications for crustal fragmentation processes. *Int J Earth Sci* (this issue)
- Kooi H, Beaumont C (1994) Escarpment evolution on high-elevation rifted margins: insights derived from a surface processes model that combines diffusion, advection, and reaction. *J Geophys Res* 99:12,191–12,209
- Kooi H, Beaumont C (1996) Large-scale geomorphology: classical concepts reconciled and integrated with contemporary ideas via a surface processes model. *J Geophys Res* 101:3361–3386
- Laerdal T, Talbot MR (2002) Basin neotectonics of Lakes Edward and George, East African Rift. *Palaeogeogr Palaeoclimatol Palaeoecol* 187:213–232
- Laslett GM, Gleadow AJW, Duddy IR (1984) The relationship between fission track length and track density distributions. *Nucl Tracks* 9:29–38
- Lisker F, Ventura B, Glasmacher UA (2009) Apatite thermochronology in modern geology. *Geol Soc London Spec Publ* 324:1–23
- Logatchev NA, Belousov VV, Milanovsky EE (1972) East African Rift Development. *Tectonophysics* 15:71–81
- MacPhee D (2006) Exhumation, Rift-flank uplift, and Thermal Evolution of the Rwenzori Mountains Determined by Combined (U-Th)/He and U-Pb Thermochronometry. Master Thesis, Massachusetts Institute of Technology
- Mbede EL (2001) Tectonic setting and uplift analysis of the Pangani Rift Basin in Northern Tanzania using apatite fission track thermochronology. *Tanzan J Sci* 27A (Abstr vol)
- McConnell RB (1959) Outline of the geology of the Ruwenzori Mountains, a preliminary account of the results of the British Ruwenzori expedition, 1951–1952. *Overseas Geol Miner Resour* 7(3):245–268
- Michot F (1938) Etude pétrographique et géologique du Ruwenzori septentrional. *Mém Inst Roy Colon Belg Sect Sc Nat Med* 8:66–271
- Mitchell SG, Reiners PW (2003) Influence of wildfires on apatite and zircon (U-Th)/He ages. *Geology* 31:1025–1028
- Montgomery DR, Brandon MT (2002) Topographic controls on erosion rates in tectonically active mountain ranges. *Earth Planet Sci Lett* 201:481–489
- Morley CK (1999) Tectonic evolution of the East African Rift System and the modifying influence of magmatism: a review. *Acta Vulcanol* 11(1):1–19
- Nagudi B, Bauer FU, Glasmacher UA, Foerster A, Foerster H-J, Schumann A, Kontny J (in preparation) Petrography and geochemistry of Rwenzori Mountains lithologies, East African Rift System, Uganda
- Noble WP, Foster DA, Gleadow AJW (1997) The post-Pan-African thermal and extensional history of the crystalline basement rocks in eastern Tanzania. *Tectonophysics* 275:331–350
- Nyblade AA (1997) Heat flow across the East African Plateau. *Geophys Res Lett* 24(16):2083–2086
- Nyblade AA, Brazier RA (2002) Precambrian lithospheric controls on the development of the East African rift system. *Geology* 30(8):755–758
- Nyblade AA, Pollack HN, Jones DL, Podmore F, Musjayandebvu M (1990) Terrestrial heat flow in East and Southern Africa. *J Geophys Res* 95:17,371–17,384
- Ollier CD, Pain CF (2000) *The origin of mountains*. Routledge, London
- Osmaston HA, Harrison SP (2005) The late Quaternary glaciation of Africa: a regional synthesis. *Quatern Int* 138:32–54
- Ovington T, Burdon P (2009) Upper Pliocene Fluvio-DELataic Reservoirs of the Victoria Nile/Butiaba Play, Alpert Rift, Western Uganda. PESGB Conference September 2009, London
- Petters SW (1991) Regional geology of Africa. In: Bhattacharji S, Friedmann GM, Neugebauer HJ, Seilacher A (eds) *Lect Notes Earth Sci* 40. Springer, Heidelberg
- Pickford M (1990) Uplift of the Roof of Africa and its bearing on the Evolution of mankind. *Human Evol* 5(1):1–20
- Pickford M, Senut B, Hadoto D (1993) Geology and paleobiology of the albertine rift valley in uganda-zaire. vol I, *Geol Occas Publ* 24 Centre International pour la Formation et les Echanges Geologiques, Orléans
- Pik R, Marty B, Carignan J, Lavé J (2003) Stability of the Upper Nile drainage network (Ethiopia) deduced from (U-Th)/He thermochronometry: implications for uplift and erosion fo the Afar plume dome. *Earth Planet Sci Lett* 215:73–88
- Pik R, Marty B, Carignan J, Yirgu G, Ayalew T (2008) Timing of East African Rift development in southern Ethiopia: implication for mantle plume activity and evolution of topography. *Geology* 36:167–170
- Reiners PW, Brandon MT (2006) Using thermochronology to understand orogenic erosion. *Annu Rev Earth Planet Sci* 34:419–466
- Reiners PW, Ehlers TA (2005) Low-temperature thermochronology: techniques, interpretations and applications. *Rev Mineral Geochem* 58:151–176
- Reiners PW, Farley KA (2001) Influence of crystal size on apatite (U-Th)/He thermochronology: an example from the Bighorn Mountains, Wyoming. *Earth Planet Sci Lett* 188:413–420

- Reiners PW, Nicolescu S (2006) Measurement of parent nuclides for (U-Th)/He chronometry by solution sector ICP-MS, ARHDL Report 1, University of Arizona
- Reiners PW, Shuster DL (2009) Thermochronology and landscape evolution. *Phys Today* 62(9):31–36
- Ring U (2008) Extreme uplift of the Rwenzori Mountains in the East African Rift, Uganda: Structural framework and possible role of glaciations. *Tectonics* 27 (TC4018). doi:[10.1029/2007TC002176](https://doi.org/10.1029/2007TC002176)
- Ring U, Betzler C (1995) Geology of the Malawi Rift: kinematic and tectono-sedimentary background to the Chiwondo Beds, northern Malawi. *J Hum Evol* 28(1):7–21
- Ring U, Betzler C, Delvaux D (1992) Normal versus strike-slip faulting during rift development in East Africa: the Malawi rift. *Geology* 20:1015–1018
- Roller S, Hornung J, Hinderer M, Ceglarek J, Ssemmanda I (2008) A Middle Miocene to Pleistocene synrift sedimentary sequence in the southern Albertine Graben (Uganda). 26th IAS Regional Meeting/SEPM-CES SEDIMENT 2008, Bochum, Abstract Volume, SDGG 58
- Schlueter T (1994) Zur Verbreitung, Fazies und Stratigraphie der Karoo in Uganda. *Berliner Geowiss Abh* E13:453–467
- Schlueter T (1997) *Geology of East Africa*. Gebr. Bortntraeger, Berlin, Stuttgart
- Shuster DL, Farley KA (2009) The influence of artificial radiation damage and thermal annealing on helium diffusion kinetics in apatite. *Geochim Cosmochim Acta* 73(1):183–196
- Shuster DL, Flowers RM, Farley KA (2006) The influence of natural radiation damage on helium diffusion kinetics in apatite. *Earth Planet Sci Lett* 249:148–161
- Sobel ER, Seward D (2010) Influence of etching conditions on apatite fission-track etch pit diameter. *Chem Geol* 271:59–69
- Spiegel C, Kohn BP, Belton DX, Gleadow AJW (2004) Integrating apatite fission track and (U-Th)/He data: the thermal evolution of rift-valley flanks in central Kenya. Abstract book, Int. Fission-track conference 2004, Amsterdam
- Spiegel C, Kohn BP, Belton DX, Gleadow AJW (2007) Morphotectonic evolution of the central Kenya rift flanks: implications for late cenozoic environmental change in East Africa. *Geology* 35(5):427–430
- Tanner PWG (1971) The Stanley Volcanics formation of Ruwenzori, Uganda. Fifteenth Annual Report of the Research Institute of African Geology, University of Leeds
- Taylor RG, Howard KWF (1998) Post-Palaeozoic evolution of weathered land surfaces in Uganda by tectonically controlled deep weathering and stripping. *Geomorphology* 25(3–4):173–192
- Torsvik TH, Gaina C, Redfield TF (2008) Antarctica and global paleogeography: from Rodinia, through Gondwanaland and Pangea, to the birth of the Southern Ocean and the opening of gateways. In *Antarctica: A Keystone in a Changing World*, Proceedings 10th Int Symp Antarctic Earth Sci, The National Academies Press, Washington, pp 125–140
- Upcott NM, Mukasa RK, Ebinger CJ (1996) Along-axis segmentation and isostasy in the Western rift, East Africa. *J Geophys Res* 101(B2): 3247–3268
- Van Damme D, Pickford M (2003) The late Cenozoic Thiaridae (Mollusca, Gastropoda, Cerithioidea) of the Albertine Rift Valley (Uganda - Congo) and their bearing on the origin and evolution of the Tangayikan thalassoid malacofauna. *Hydrobiologia* 498:1–83
- Van der Beek P, Mbede E, Andriessen P, Delvaux D (1998) Denudation history of the Malawi and Rukawa Rift flanks (East African Rift System) from apatite fission track thermochronology. *J Afr Earth Sci* 26:363–385
- Wagner GA (1972) Spaltspurenalter von Mineralen und natürlichen Gläsern: eine Übersicht. *Fortsch Miner* 49:114–145
- Wagner GA, Van den Haute P (1992) Fission-track dating. Enke, Stuttgart
- Wagner M, Altherr R, Van den Haute P (1992) Apatite fission-track analysis of Kenyan basement rocks: constraints on the thermotectonic evolution of the Kenya dome. A reconnaissance study. *Tectonophysics* 204:93–110
- Wallis CS, Valliant WW (2004) Technical report on the Kilembe Mine, Uganda. Prepared for Uganda Gold Mining Ltd. Rosco Postle Associates Inc, Report
- Wallner H, Schmeling H (2010) Rift induced delamination of mantle lithosphere and crustal uplift. *Int J Earth Sci*, doi:[10.1007/s00531-010-0521-6](https://doi.org/10.1007/s00531-010-0521-6)
- Whittow JB (1966) The landforms of the central Ruwenzori, East Africa. *Geogr J* 132(1):32–42
- Wolf RA, Farley KA, Silver LT (1996) Helium diffusion and low-temperature thermochronometry of apatite. *Geochim Cosmochim Acta* 60(21):4231–4240